# MODELLING ADHESION IN PACKAGING MATERIALS
Physical Tests and Virtual Tests in Abaqus

HANNA BRUCE and CHRISTIAN HOLMQVIST

Master's Dissertation

MODELLING ADHESION
IN PACKAGING MATERIALS

Physical Tests and Virtual Tests in Abaqus

HANNA BRUCE & CHRISTIAN HOLMQVIST

Supervisor: **KENT PERSSON**, PhD; Div. of Structural Mechanics, LTH, Lund.
Examiner: **PER JOHAN GUSTAFSSON**, Professor; Div. of Structural Mechanics, LTH, Lund.

Abstract

The adhesive properties in packaging material have been simplified for a long time. As more advanced packages are developed the correct mechanical properties for the adhesive strength is needed to make packages cost efficient and reliable.

The problem today is that no good evaluation technics have been developed for determining the mechanical properties of adhesives. Different test methods for determining adhesion was studied. Peel tests were found most suited and were used when performing experimental tests on the package material. The purpose of the experimental tests were to evaluate the mechanical adhesion properties. FE-simulations were done to replicate the experimental peel tests with the aim of determining the correct adhesion properties needed in simulations. ABAQUS/Standard was used for the FE-simulations.

It was found that it is difficult to evaluate the properties needed by only using peel tests. It was also found that it is possible to match the peel force from experimental tests with the peel force from FE-simulations. It is hard to say if the correct properties were used since many combinations yields the same peel force. Not only the adhesion parameters affects the result. If the goal is to fine tune the adhesion parameters in simulations, then all other parameters should be validated first. As an example, it is critical that the correct material models are used.

The conclusion is that there is still a great research need before a method for evaluating adhesion strength is developed. With new experimental test methods and correct material models, good estimations of the adhesion properties could be made. This study brings up topics that further studies on adhesion would need to address.

Contents

Chapter 1

Introduction

1.1 Background

Changing the dimension of a layer in the packaging material is expensive and it is uncertain if the new composition meets the high standards of Tetra Pak. It is a long and tedious process to produce package material, run the filling machine and verify and validate a new package material variant. Money can be saved if FE-analyses can be made to verify a new composition before it is produced. It is of great importance that a FE-analysis is accurate and reliable; otherwise it can be misleading and a waste of time. It is important that the input variables are proved and verified to make a simulation reliable. As technology advances; the analysis possibilities of the FE-method increases. To remain in the forefront it is important to explore these new areas. An area in which there still is a lot to explore is implementation of adhesion strength in FE-simulations.

A real problem that can be solved by implementing correct adhesion is the opening mechanics of certain type of packages. Layers of aluminum and polymer cover the opening of the package and these layers are cut when the cap is turned. The adhesion strength should be high enough to prevent the aluminum foil and polymer layers to separate during opening. Another problem that could be more thoroughly studied is when the package material is creased and folded.

1.2 Objectives

The objective of this thesis is to take the first step towards a verified method for incorporating adhesive strength in FE-simulations. This will be done through experimental tests on packaging materials with different geometries which will be recreated in ABAQUS/Standard to fine tune the adhesive parameters. When simulations with the same adhesion properties correspond with different experimental tests; the adhesion strength is verified.

1.3 Problem formulation

Measuring mechanical adhesive properties of thin materials is a difficult task. An investigation of the test methods used at Tetra Pak today will be done. If found that they do not provide sufficient information for evaluating the parameters needed for simulating the adhesion, other test methods will be suggested.

The adhesion strength between layers in the material is a relatively unexplored area. The effects of different geometries in the material on the adhesive release mechanism are to be studied. A study of how the different input parameters for modelling adhesion affects the final result will also be performed. A method for evaluating the physical tests and determination of the properties of the adhesion is the long term goal.

1.4 Scope and Delimitation

The adhesion at the two different sides of the Aluminum layer will be studied. No in-depth analyzes of how the seperation rate affects the adhesion will be performed.

The theory presented will be focused on theory with connection to adhesion or the discussed problems. FE and large displacement theory can be found in [1] and [2].

Chapter 2

Adhesion

2.1 Adhesion

Between substances in intimate contact, intermolecular forces arise causing attraction. This attraction is called adhesion. Cohesion concerns the intermolecular forces within a material. In both cases the intermolecular forces are mainly van der Waals forces, [3].

To begin with, it is necessary to clarify the difference between practical and fundamental adhesion. Practical adhesion relates to the force needed to break an adhesive bond and is measured in fracture energy, G, or fracture stress. Fundamental adhesion on the other hand relates to the forces and mechanisms holding the parts of an adhesive bond together. In the 1920s studies concerning fundamental adhesion took off with the work of McBain and Hopkins, [3]. In the early years of adhesion studies the discovered mechanisms were thought of as contradictive and not of as mechanisms that could work alongside, [3].

More about the intermolecular forces and other mechanisms of adhesion can be read further on in this chapter. First a short review of the parts and the structure of an adhesive joint will be given.

2.1.1 Adhesive joints

An adhesive is a material that can join other materials together when applied to their surfaces, [6]. The adhesives first used by humans came from plants and animals. In the 1940s synthetic polymers were introduced. Today they are used in as good as all industries since they effectively join different types

of materials and contribute to strong joints, [3]. The adhesive, which is liquid, join the solids, called adherends, together, [7]. Before they are part of the joint the solids can be called substrates, [6]. The adhesive has to be liquid to ensure good molecular contact between the adhesive and the substrate by wetting the surface properly. Before adding the adhesive a primer can be used to protect the substrate surface or to improve the adhesion. Heat can be applied to get the adhesive to harden. When the adhesive and adherend bond, a zone called the interphase forms. The interphase has characteristic properties that differ from those of the adhesive and the adherend, which affects the mechanical properties of the joint, [3] and [7]. The interface is the contact boundary between the adhesive an adherend. The interface is within the interphase. The strength of adhesive interfaces changes over time due to environment and surrounding conditions as do the strength and durability of the whole joint,[3] and [7].
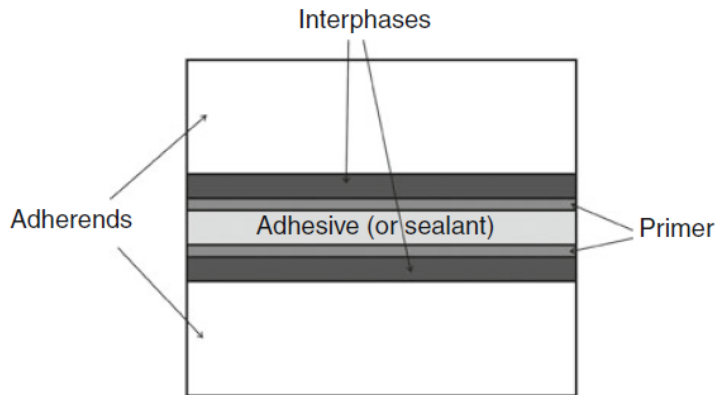
Figure 2.1: The parts of an adhesive joint [3].

The adhesive is often a monomer that polymerizes during the hardening process. Pressure sensitive adhesives stays in the viscoelastic state and remains sticky, [3] and [6]. Polymeric adhesives are good when bonding materials with different thermal expansion properties, due to that they are flexible. They are good when bonding thin plates. They provide good damping properties giving high fatigue strength. They provide a uniform stress distribution which results in possibilities for high loads to be transmitted and to have high stiffness. Polymers are sensitive to extreme humidity and temperatures.

Sealants, similar to adhesives, have the purpose to bond substrates together. The difference is that sealants are used to form a protective layer at the same time as the surfaces are bonded, [3].

2.2 Determining the adhesion with fracture energy or fracture stress

The fracture energy and the fracture stress can both be used when expressing the adhesion.

The relation between the practical adhesion, G, and the fundamental adhesion, G_0, can in a simple way be described by

$$G = G_0 + \Psi \tag{2.1}$$

G_0 is equal to W_A, the work of adhesion, if failure occurs at the interface between the phases and to W_C, the work of cohesion, if the failure is cohesive. W_A and W_C are available surface energies. W_A and W_C are given by the Dupre equations.

$$W_A = \gamma_1 + \gamma_2 - \gamma_{12} \tag{2.2}$$

$$W_C = 2\gamma_1 \tag{2.3}$$

Where γ_1 and γ_2 are the surface energies for the two materials and γ_{12} is the interfacial energy. Eq. 2.2 and 2.3 are thermodynamic and reversible, but this does not hold for adhesive bonds, [4]. The fracture of an adhesive joint can occure in the substrate, at the interface or in the adhesive. G_0 may therefore be expressed in a weighted average for these three possibilities.

$$G_0 = iG_0(interfacial) + b'G_0(adhesive) + sG_0(substrate) \tag{2.4}$$

i , b' and s are area fractions, with the sum 1, [6].

Ψ is the collection of other energy demanding processes that occurs during breaking of an adhesive bond, [4]. This energy is for example dissipated viscoelastically or through plastic deformations. Following relation has been shown

$$\Psi = G_0 f(\dot{a}, T, \epsilon) \tag{2.5}$$

Thus giving that the fracture energy depends on the temperature, the rate of the crack growth, and the strain level, [6]. Ψ is much greater than G_0. The terms, G and G_0, are coupled, and in very simple cases proportional, [4].

The work of adhesion depends on in which fluid medium the joint is formed. Usually it is air. If the air contains water vapor or if the adhesive is volatile, vapor will be absorb to the surface of the adherend. This has to be taken into consideration since this will lower the surface energy of the adherend. The reduction of the energy is at equilibrium called the equilibrium spreading pressure. For more about this see [7].

The practical adhesion can be expressed in fracture stress using the following equation

$$\sigma_f = k(EG/l)^{\frac{1}{2}} \qquad (2.6)$$

k is a constant, l is the length of the critical crack and E is the effective modulus, [4].

More about fracture mechanics and fracture of adhesive joints is found in chapter 3.

2.3   Mechanisms of adhesion

There are different types of forces acting across the interface adhesive/ substrate. These forces, or mechanisms of adhesion, are explained by a number of theories. The number of theories differs between sources. Kinloch mentions four mechanisms of adhesion. These are; mechanical interlocking, diffusion theory and electronic theory. J. Comyn includes chemical bonding and weak layer boundary theory as well, [11].

The intimate contact between molecules across the interface gives rise to so called adsorption forces. These are always present in adhesive bonds unlike the forces described by the other theories, which are dependent on the case studied. In the case of an adhesive bond the factors that affects the spreading and wetting of the substrate surface by the liquid adhesive is of great importance. This holds for all of the theories.

2.3.1   Adsorption theory

The type of attraction forces between the materials depends on the chemical nature of the surfaces. The bonds can be of secondary or primary type.
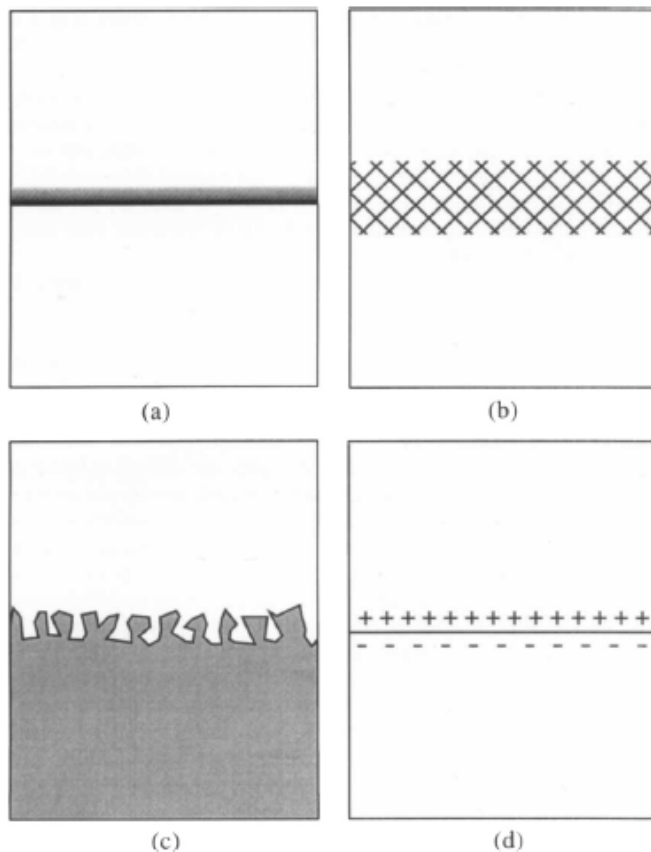
Figure 2.2: Illustration of a) Adsorption theory b) Diffusion theory c) Mechanical theory d) Electrostatic theory [7].

The relative strength of a primary bond is higher than for a secondary bond. Donor-acceptor bonds has been suggested to occur and their strength is between that for primary and secondary bonds, [6].

Van der Waals forces are the most common type of intermolecular forces. Van der Waals forces are divided into dispersion forces and polarization forces. Permanent dipoles and electric fields of nearby charges cause these forces, [5]. Dispersion forces are the weaker of the two but exist in all materials. Dispersion forces, also called London forces, arise due to attraction between instantaneous dipoles. These dipoles are caused by internal electron motions, [6]. Polymers are asymmetric and the exact dispersion interaction energy is difficult to calculate.

Londons equation which gives the interaction energy for the dispersion is given by

$$E_{ii} = \frac{-3(\alpha_1\alpha_2)^2 I_1 I_2}{2(I_1 + I_2)r^6} \tag{2.7}$$

were α_1 and α_2 are the polarizability of the molecules and I_1 and I_2 are the ionization potentials, [11].

Polymers are asymmetric and the exact dispersion interaction energy is difficult to calculate, Londons equation can not be used. It can not be used for large molecules either, diameter $> 0{,}5$ nm. The large distance results in a retardation effect and the dispersion energy drops with $1/r^7$ instead, [5]. Polarization forces arise between permanent dipoles, called Keesom orientation forces, and the potential energy is given by

$$E_{pp} = \frac{-2\mu_1^2\mu_2^2}{3kT(4\pi\epsilon_0)^2 r^6} \tag{2.8}$$

were μ_1 and μ_2 are the dipole moments and ϵ_0 is the permittivity of a vacuum, k is Boltzmann's constant and T is the absolute temperature, [11]. Polarization forces can arise between a permanent dipole and an induced dipole, called Debye forces. The Keesom orientation interaction energy is temperature dependent and the potential energy is given by

$$E_{pi} = \frac{-\mu_1^2\alpha}{4\pi\epsilon_0 r^6} \tag{2.9}$$

were μ_1 is the moment of the permanent dipole, E is the electric field and α is the polarizibility of the non-polar molecule, [11].

The total van der Waals free energy is the sum of the contributions from the above mentioned three types, [5].

The value of both dispersion and polarization forces falls rapidly with the distance between the molecules. This results in that only the molecules in the top layer of the surface are affected by these forces, [11]. For polymers and molecules with greater diameter than 0.5 nm the London dispersion energy falls more rapid than for spherical molecules due to a delay in the propagation of the electromagnetic wave, caused by the larger distance between the molecules, [5].

Van der Waals forces are also called secondary bonds, [6].

By summing the energy for all atoms in two bodies the contribution from van der Waals forces to the interaction energy can be calculated, [5].

The donor-acceptor bonds may be included in the secondary bonds. The acid-base interactions that act across the interface are an important contribution to the intrinsic adhesion forces, [6]. It was Lewis who in the 1920s introduced the theory of electron-pair bond. The acid and the base share a pair of electrons, which are initially electrons of the base. When the electrochemical nature of the two molecules starts to differ more and more an ion is formed, [5]. The strength of the acid-base interactions can be described by their heats of reaction, the enthalpy, [11].

Hydrogen bonds are a type of acid-base interactions, [6].

To the category primary bonds are the chemical bonds; ionic, covalent and metallic interfacial bonds, counted. The chemistry of the interface affects which bonds that are formed, [6]. Often when high level of adhesion is required covalent bonds have to be present. For strong adhesive bonds it is important that the stress can be transferred across the interface. The creation of primary bonds, in form of coupling chains, at the interface can contribute to this. These types of chains could be placed at the interface or if the materials are mixable chains can interdiffuse, both ways strengthens the adhesive bond, [5].

2.3.2 Mechanical theory

In the 1920s McBain and Hopkins claimed that "a good joint must result whenever a strong continuous film of partly embedded adhesive is formed in situ". In their work, in which they also discussed adsorption theory, they called this the Mechanical theory, [4]. This theory can be referred to as Mechanical interlocking in some literature.

If the substrate surface contains irregularities the adhesive enters these before the hardening of the adhesive starts. This theory contributes to the adhesion forces when the materials are of porous type, [11].

A rough surface has atoms bonding with fewer neighboring atoms than atoms on a smooth surface have, see figure 2.3. This results in a higher surface energy, G_0-value, for a rough surface. G_0 is given per unit area and for a rough surface the true area is greater than for a smooth surface giving a higher G_0-value, [4].

For some surfaces the true area is indefinitely large. In these cases failure will occur cohesively since the interface will be strong.
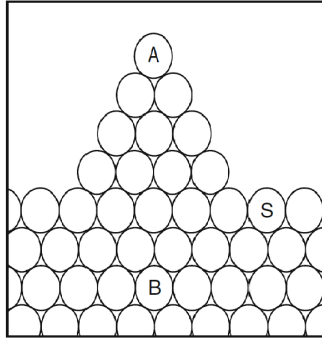
Figure 2.3: The surface around S is smooth and S bonds fewer atoms than A. This is why rough surfaces have higher surface energy than smooth surfaces [4].

In the 1950s and the 1960s studies on adhesion between smooth surfaces and adhesion between surfaces with different roughness were performed. The results made the contribution from the mechanical interlocking to the interfacial forces questionable. Good adhesion could be obtained between smooth surfaces and a rougher surface did not always result in a stronger joint. This can be explained by the fact that it can be difficult to obtain good wetting of rough surfaces, [4] and [6]. If the wetting of the surface is good the opposite result is obtained. A rougher surface then gives a stronger joint and mechanical interlocking then contributes to the adhesion, [4].

The surface roughness of the substrate can be increased with pretreatment, mechanical or chemical. Mechanical pretreatment does not create irregularities at the surface that contributes to the mechanical interlocking but chemical pretreatment does. Mechanical pretreatment still results in stronger joints. This is due to that it ensures better wetting of the surface by removing contaminations and because weak boundary layers are removed. More about weak layers in section 2.3.6. Roughening results in a greater area of the surface. When using chemical pretreatment it has to be ensured that the interface does not become too weak, [6].

2.3.3 Chemical bonding theory

The chemical bonding theory brings up the formation of ionic, covalent or hydrogen bonds across the interface. J. Comyn brings this up as a separate theory, [11]. Others, for example Kinloch, brings this theory up in the adsorption theory. This has already been described and can be found in section 2.3.1.

2.3.4 Electronic theory

The electrostatic theory was formulated in the 1940s, in the Soviet Union, by Deryaguin and colleagues and it involves Coulombic attraction across the interface, [4]. The interface is treated as an electrical capacitor in this theory. A double layer of electrical charge, at the interface, will be the result of electronic or ionic charge moving across the interface due to electrochemical potential difference. Such a difference exists between all materials in contact since all condensed materials contains free charges. A potential difference occurs and increases when the parts of the capacitor are separated, finally discharge occurs, as during joint failure. Deryaguin states that these electrostatic forces contribute to the intrinsic adhesion. This has been questioned and it has been suggested that they are a result of high joint strength instead, [6].

The energy needed to separate the interface is given by

$$A_0 = \frac{h_c \epsilon_d}{8\pi} \cdot \left(\frac{dV_c}{dh_c} \right)^2 \tag{2.10}$$

V_c is the discharge potential at the discharge gap and h_c and ϵ_d are dielectric constants. The value of A_0 is too large. This is because the in peeling tests measured energy dissipated through viscous and viscouelastic response of the material should not be included, [6].

The peel energy is dependent on the rate of separation, as is the work of separation of the plates for a capacitor, [4]. The work of separation for a capacitor depends on the gas pressure, and this is sometimes the case for measured peeling energy.

The electrostatic theory is not always applicable. For polymers, which are insulators, it is difficult to apply, [11]. There are different views on the size of the contribution from electrostatic to adhesion. According to [4], the most common view is that the contributions are likely to be small. For small particles it is of relevance. The charged particles can be influenced by electrical fields and thereby be precipitated.

2.3.5 Diffusion theory

The diffusion theory is based on that mutual diffusion of polymer chains across the interface gives rise to intrinsic adhesion. Both autohesion, when two films of the same polymer are joined together, and interdiffusion between/of two different polymers are considered, [6]. The theory was put

forward in the Soviet Union in the 1950s, at approximately the same time as the electrostatic theory, by S.S. Voyutskii and his colleagues. Voyutskii argued for it to be applicable on adhesion between metals and polymers. To begin with the theory was not accepted by those who supported the adhesion theory. Autohesion and interdiffusion between similar polymers got acceptance in 1970, [4].

Interdiffusion can occur between polymers in contact. The polymers have to be mobile and compatible, meaning they have to be mutually soluble. That polymers have similar structure is not a guarantee that they are compatible, most polymers are incompatible, [11].

The compatibility between two polymers can be determined using the solubility parameter δ_s

$$-\delta_s = \left(\frac{\Delta H_v - RT}{V} \right)^{\frac{1}{2}} \tag{2.11}$$

ΔH is the molar heat of vaporization, R is the gas constant, T temperature in Kelvin and V is the molar volume.

The polymer has to be amorphous when being mixed with a solvent. If crystalline the free energy makes it resistant to dissolving, [6].

Thermodynamic criteria can also be used when determining if two polymers are compatible. If Gibbs free energy of mixing, given by

$$\Delta G_m = \Delta H_m - T \Delta S_m \tag{2.12}$$

is negative then the polymers are compatible. ΔH_m is the enthalpy of mixing and ΔS the entropy of mixing.

The Flory-Huggins theory gives the free energy of mixing as

$$\Delta G_{mix}/kT = \chi \phi_1 \phi_2 + (\phi_1/x_1) ln \phi_1 + (\phi_2/x_2) ln \phi_2 \tag{2.13}$$

ϕ is the volume fraction, for polymer 1 and polymer 2 respectively, and x the degree of polymerization. χ is the, temperature dependent, Flory-Huggins interaction parameter, k Boltsmann's constant and T the absolute temperature. This theory considers the number of ways in which chain segments of the polymers may be distributed among identical unit cells in a hypothetical

lattice. The first term expresses the enthalpy of mixing and the last two the entropy of mixing, [4].

Voyutskii's theory and experimental evidence on that time, temperature, polymer type, molecular weight and viscosity effects the joint strength the way a diffusion process would was strengthened by Vasenin. Using Fick's second law, which describes build-up or decay of diffusing species, he modeled the penetration depth of polymeric chains into a polymeric substrate.

$$l_p = \frac{(\pi D_d t_c^{\frac{1}{2}})^{\frac{1}{2}}}{k_3} \qquad (2.14)$$

l_p is the deduced depth, due to the reduction of D_f, the diffusing constant, with time. D_f is given by

$$D_f = D_d t_c^{-\beta} \qquad (2.15)$$

D_d a constant describing the mobility of the macromolecules, t_c the time of contact and β, also a constant, describes the rapidity of change of D_f and is 0.5. k_3 in eq. 2.11 describes the stiffness, bond length and valency angles along the polymeric molecules and is a constant. The peeling energy is given by

$$P = k_4 (\frac{2N_\rho}{M})^{\frac{2}{3}} D_d^{\frac{1}{2}} t_c^{\frac{1}{4}} \qquad (2.16)$$

Where the second term is the number of chains crossing the phase boundary. k_4 is a constant given by the characteristics of the polymers. N is Avogadros number, ρ the density and M the molecular weight of the polymer. This model does not take the viscoelastically and plastically dissipated energy into account. The viscoelastic and plastic contributions are likely to be contained in the constants since they were determined by fitting the equations to the experimental data.

Macromolecules does not have to interpenetrate deep to give a large increase in joint strength as long as they can create an entanglement network structure, [6].

The kinetics of wetting may be effected by the time of contact and the molecular weight since they can give an increasing interfacial contact. This gives rise to secondary forces, van der Waal forces, and some workers, for example

Anand, mean that this is the reason why joint strength depends on contact time and molecular weight. Regarding autohesion they believe that the inter-diffusion does contribute to the intrinsic adhesion but that its contribution is small.

When plastics, with similar solubility parameters, are welded together inter-diffusion does affect the intrinsic adhesion. A solvent, that plasticizes the polymers, or heat gives the polymer chains the mobility they need to inter-diffuse. Kinloch does not consider the penetration of polymer molecules into metal surfaces as an example of the diffusion theory. The increase in the intrinsic adhesion is mainly caused by the fact that the polymer gives improved adsorption on the metal surface, [4].

2.3.6   Weak boundary layer theory

Contaminants can cause a cohesively weak layer, which wetting properties most likely are bad, resulting in a weak joint. The name interphase is some-times used for this weak layer. All surfaces are contaminated to some ex-tent, even metal surfaces that often are thought of as clean. A joint be-comes stronger if the substrate has high surface energy since this aids wet-ting and gives a higher fracture energy. Pretreatment is therefore almost always needed. Even if it does not make the surface molecular clean the adhesive bonds becomes stronger. The adhesive can in some cases dissolve the contaminants, [4] and [11].

Most polymers and elastomers have additives added to them to change their properties. Most polymer-additive solutions are incompatible and thermody-namically unstable, in the way that the additive migrates out of the polymer. A weak boundary layer can be formed when a polymeric adhesive solidify since additives with low molecular weight migrates to the interface. This type of migration, of low-weight molecules, can take place in the polymer itself and during the bonding process.

Bikerman and collegues studied weak boundary layers in the 1950s and 1960s. He claimed that the existence of weak boundary layers is widespread. Addi-tionally he claimed that failure close to the substrate-adhesive is of cohesive type in the weak boundary layer and not of adhesive type. Now it has been proven that adhesive failure does occur, but are not common. Cohesive fail-ure close to the interface can occur without the existence of a weak boundary layer. Finally Bikerman claimed that the rheology of the joint determines the strength of the adhesive bond, which is true, and not the forces acting across the interface, which is wrong, [4].

Chapter 3

Fracture mechanics

Fracture mechanics are used when studying failure of materials. Originally continuum fracture mechanics, which consider a structure with a flaw, considered as an elliptical crack, were developed for cohesive fractures, [6]. Today fracture mechanics theories are used in for example the areas of adhesive joints, dynamic fracture problems and composite materials although they were originally developed for cohesive failure. The basic assumption in fracture mechanics is that fracture occurs due to the existence of voids or flaws. For adhesive joints this can be for example bubbles of trapped air, additive particles or inhomogeneities in the adhesive. When applying stress that is higher than a critical value these form cracks that propagate, resulting in fracture. The defects propagate due to the stress concentration close to the crack tip, [12].

3.1   Modes of fracture

There are three principal modes of fracture, they are shown in figure 3.1. They were introduced by Irwin who was one of the first to study cracks, [13].

Mode I is a tensile normal mode or cleavage mode. It can be caused by peel or cleavage forces. Mode II is a shearing or sliding mode, with shearing along a plane. Mode III is also a shearing mode or twisting mode. The shearing is out-of-plane, along an axis, [11]. Combinations of these three modes are possible. Mode I is the most common fracture mode in engineering applications which for isotropic materials is the mode with the lowest fracture energy. The crack will propagate normal to the maximum principal stress, [12].
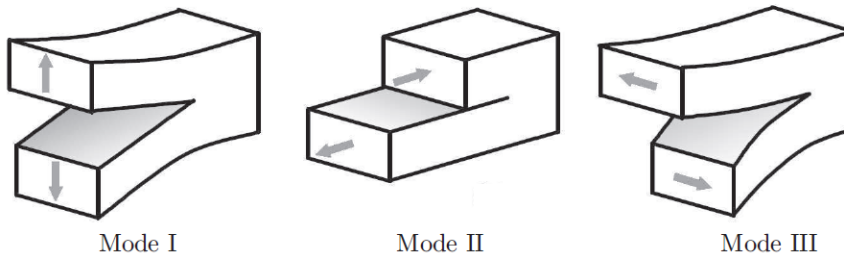
Figure 3.1: Modes of failure, [14].

There are differences between brittle and ductile systems. For a brittle system in Mode I loading, microcracks occurs in front of the crack tip. When uniting and growing the crack propagates. For ductile systems plasticization in the crack tip zone precedes the crack propagation, [14].

When considering adhesive joints the load is often a mixed-mode between Mode I, II and III, due to that the crack often is constrained to the adhesive layer or along the interface, regardless of the orientation of the adhesive layer to the applied loads, [12].

Rigid adhesives are in general weak in Mode I but strong in the other two whereas rubbery adhesives are strong in Mode I but have a higher creep rate in the other two, [11].

3.2 Linear Elastic Fracture Mechanics- LEFM

If the material behavior can be assumed to be linear elastic, Linear Elastic Fracture Mechanics, LEFM, can be used to predict delamination growth. An energy balance approach can be used and the crack growth criterion is then said to be global since a quite large material volume is involved. Another approach is to analyse the stress state at the crack tip to predict the crack propagation. A stress intensity factor is then used. Using this method the crack growth criterion is said to be local since only the small volume around the crack tip is studied, [13].

A plastic zone develops in front of the crack tip. Its area can be determined using yield criterias. If small enough, Small Scale Yielding (SSY), LEFM can be used. In theory, with a linear material model, the stress at the crack tip is infinite, [13] and [14].

3.2.1 Energy balance approach

When predicting the propagation of a crack an energy balance approach can be used. The Griffith criterion states that the crack will propagate when the amount of energy is enough to create new crack surfaces, [13]. Griffith published the pioneering papers on the subject in 1920, [14]. In 1956 Irwin introduced the energy release rate G and an approach equivalent with Griffiths but better suited for engineering problems. G is a measure of the available energy for an increment of crack extension, [15].

The energy balance for a constant volume can be written

$$\frac{\partial U_e}{\partial A} = \frac{\partial U_d}{\partial A} + \frac{\partial U_s}{\partial A} + \frac{\partial U_k}{\partial A} \tag{3.1}$$

$$G = \frac{\partial U_e}{\partial A} - \frac{\partial U_s}{\partial A} - \frac{\partial U_k}{\partial A} \tag{3.2}$$

Where U_e is the input energy, U_k is the kinetic energy, U_s the stored energy and ∂A the increase in area for the propagating crack. U_d is the dissipated energy, the energy used for crack propagating and is called G. When G reaches the critical value G_c and $\partial G/\partial A > 0$ crack propagation is initiated. G_c is a material parameter. The kinetic energy is negligible for stable static tests and this can be used when deriving G_c, from eq. 3.2, for linear-elastic materials

$$G_c = \frac{1}{2} P^2 \frac{\partial C}{\partial A} \tag{3.3}$$

and power-law materials

$$G_c = \frac{1}{n+1} \left(nP \frac{\partial u}{\partial A} - u \frac{\partial P}{\partial A} \right) \tag{3.4}$$

u is the displacement of the material in the direction of the force, C is the compliance, $C = u/P$, and n is the power-law index $C_n = u_n/P$. P is the load at the onset of the crack propagation, [12]. For a cracked body eq. 3.3 and 3.4 is valid both for fixed-extension and constant-load conditions. Also it is not only restricted to LEFM. It holds even for rubbers which has significant internal energy dissipation outside the intermediate crack tip regions. The stored strain energy that can be used for crack propagation should in this case be taken as the input energy minus the loss energy. The energy

balance approach makes it possible to predict an unambiguous value of G_c independent of the crack location, i.e if it is close or at the interface or in the adhesive layer, [6].

3.2.2 Stress intensity approach

Another approach is to analyse the stress field at the crack tip to predict crack propagation. Two cases are studied; a crack located far from the interface, in the bulk material, and secondly a crack located near the interface. For an elastic body the stress intensity factor around the crack, in polar coordinates r and θ, is calculated with

$$\sigma_{ij} = \frac{C_1}{\sqrt{r}} f_{1ij}(\theta) + \sum_{n=0}^{\infty} C_n r^{(n-1/2)} f_{nij}(\theta) \tag{3.5}$$

At the crack tip the first term, the singular term dominates, [12]. These stress function solutions are developed by Westergaard, [6]. Irwin introduced the material independent stress field parameter K, the stress intensity factor. It can uniquely define the stress field around a sharp crack in a linear elastic material. With

$$C_I = \frac{K}{\sqrt{2\pi}} \tag{3.6}$$

$$K_I = \sigma_0 \cdot \sqrt{2\pi a} \tag{3.7}$$

where σ_0 is a remote stress perpendicular to the crack, which has length $2a$, the stress close to the crack tip can be written

$$\sigma_{ij} = \frac{K}{\sqrt{2\pi r}} f_{ij}(\theta) \tag{3.8}$$

When K reaches the critical value K_c, called the fracture toughness, fracture occurs. K_c is a measure of a material property, [6]. The stress alone is not a reasonable fracture criterion since the stress at the crack tip becomes infinite, when $r \to 0$. The stresses at the crack tip for Mode I loading becomes

$$\sigma_{xx} = \frac{K_I}{\sqrt{2\pi r}} \cos \frac{\theta}{2} (1 - \sin \frac{\theta}{3} \sin \frac{3\theta}{2}) \tag{3.9}$$

$$\sigma_{yy} = \frac{K_{\mathrm{I}}}{\sqrt{2\pi r}} \cos\frac{\theta}{2}(1 + \sin\frac{\theta}{3}\sin\frac{3\theta}{2}) \tag{3.10}$$

$$\tau_{xy} = \frac{K_{\mathrm{I}}}{\sqrt{2\pi r}} \cos\frac{\theta}{2}\sin\frac{\theta}{3}\sin\frac{3\theta}{2} \tag{3.11}$$

Rewriting the expression for the stress intensity factor in Mode I loading using Q, a geometry factor, gives

$$K_{\mathrm{I}} = Q\sigma_0\sqrt{a} \tag{3.12}$$

Q is a non-dimensional function of crack length and structural geometry, [12]. Through experiments or theoretically it is possible to determine the value of Q, see Kinloch [6]. The expressions for Mode II and III becomes

$$K_{\mathrm{II}} = Q\tau_{\mathrm{II}}\sqrt{a} \tag{3.13}$$

$$K_{\mathrm{III}} = Q\tau_{\mathrm{III}}\sqrt{a} \tag{3.14}$$

The stress state at the crack tip changes with the width of the specimen and therefor does G_{Ic} and K_{Ic} so too. When ϵ_z is zero the fracture condition is plane strain and when σ_z is zero it is plane stress. Plane strain results in a lower value for G_{Ic} and K_{Ic} due to the limited plasticity at the crack tip. When designing plane strain is used not to overestimate the failure load, [12]. When LEFM is applicable G_c and K_c may be related. The relationship between G and K depends on whether plane stress or plane strain is the state. The three stress states can exist at one time and therefore G_c in plane strain can be written

$$G_C = \frac{K_{\mathrm{I}}^2}{E}(1 - \nu^2) + \frac{K_{\mathrm{II}}^2}{E}(1 - \nu^2) - \frac{K_{\mathrm{III}}^2}{E}(1 - \nu^2) \tag{3.15}$$

For plane stress
$$EG_i = K_i^2 \qquad i = \mathrm{I, II, III} \tag{3.16}$$

These expressions are valid for a crack in an adhesive as well, if located quite far from the interface. E is then set to E for the adhesive and G and K is G and K for the joint.

If the crack in the adhesive is located at or close to the interface the stress state is more complicated to describe. When the joint is subjected to tensile normal load, both normal and shear stresses will occur at the crack tip; likewise for the case of pure shear loading. Both K_{Ii} and K_{IIi} are needed to describe the stress state. The index denotes that the crack is at the interface. What makes it complicated is that these parameters do not have a clearly defined physical significance as for the above case. As for the case of bulk material the singular behavior of the stresses are proportional to the inverse square root of the distance r. In this case though the stresses oscillates close to the crack tip and tend to change sign with increasing frequency. The expression for the local stresses contains a logarithmic term of r giving that the crack tip stresses depends on the measuring units of r. K_{Ii} and K_{IIi} is for a tensile load given by

$$K_{\mathrm{Ii}} = \sigma_o \frac{\sqrt{2\pi}[\cos{(\zeta ln2a)} + 2\zeta \sin{(\zeta ln2a)}]}{\cosh{(\pi\zeta)}} \sqrt{a} \qquad (3.17)$$

$$K_{\mathrm{IIi}} = \sigma_o \frac{-\sqrt{2\pi}[\sin{(\zeta ln2a)} + 2\zeta \cos{(\zeta ln2a)}]}{\cosh{(\pi\zeta)}} \sqrt{a} \qquad (3.18)$$

with a crack of length $2a$. The second term in eq. 3.17 can be replaced with Q_{Ii} and the second in eq. 3.18 with Q_{IIi}.

There are now two geometry factors. These can be functions of biomaterial constants. It is difficult to calculate the contributions from Mode I and Mode II independently of each other since they contain a logarithmic term of the dimensional parameter a. The stress intensity factors have to be combined in the fracture criterion. A combined interfacial intensity stress factor has been suggested, expressed by

$$K_{\mathrm{ic}} = \sqrt{K_{\mathrm{Iie}}^2 + K_{\mathrm{IIie}}^2} \qquad (3.19)$$

The dependence upon the units of the length parameter a, disappears due to the root. The stress intensity factor approach has more difficulties than the energy balance approach. The interface may affect the stress field at the crack tip even if the crack is located in the center of the adhesive. The relation between G and K is not as simple as when the crack is located far from the interface. It has been suggested that the E-modulus for the interface should be a weighted value of the E-modulus for the substrate, E_s, and the adhesive, E_a, [6].

For cracks near the interface it is hard to predict the relation. A value between that for when the crack is at the interface and that for the crack being far from the interface is to be expected, [6].

3.2.3 Plastic zone

A plastic zone develops at the crack tip due to the high stresses. The size and shape of the deformation zone at the crack tip depends on the stress mode. For the shear modes, Mode II and III, the decay of the stress field is slower resulting in a greater deformation zone in these cases, [14]. If the plastic zone is small enough, corrections can be made to make LEFM applicable. Irwin suggested that, when considering the crack plane $\Theta = 0$, a material which is elastic up to when the uniaxial yield stress is reached can be approximated as a circle as a first approximation. The radius of the circle is given by [15] as

$$r_y = \frac{1}{2\pi}\left(\frac{K_{\mathrm{I}}}{\sigma_{ys}}\right)^2 \tag{3.20}$$

For plane stress yield occurs when $\sigma_{yy} = \sigma_{YS}$, [15]. The radius in plane strain is given [6] as

$$r_y = \frac{1}{6\pi}\left(\frac{K_{\mathrm{I}}}{\sigma_{ys}}\right)^2 \tag{3.21}$$

The second order approximation is given in [15], with the radius r_p as

$$r_p = \frac{1}{\pi}\left(\frac{K_{\mathrm{I}}}{\sigma_{ys}}\right)^2 \tag{3.22}$$

For plane strain $r_p = 2r_y$.

In Irwins model the zone is smaller in plane strain than in plane stress. This is due to that the yield stress is higher for plane strain which gives a higher constrain at the crack tip.

In 1960 Dugdale and Barenblatt presented a plastic zone analysis in which the zone has a strip-like shape, [13]. The calculation yields for plane stress, non-hardening material and with the requirement that the stresses are finite outside the plastic zone. The solution is given by superimposing two elastic solutions that acts on half the crack length, $a + r_p$. The cases are a crack
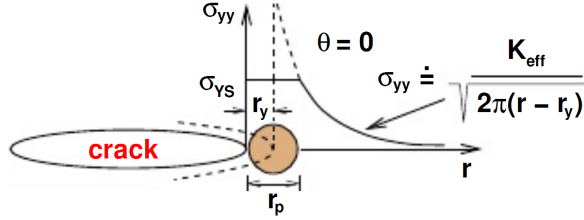
Figure 3.2: The plastic zone according to Irwin, [15].

under tension load σ and a crack with closure stress, σ_y, at the tip. The length of the plastic zone is given in [13] as

$$r_p = \frac{\pi K_I^2}{8\sigma_y^2} \tag{3.23}$$

The strip-model by Dugdale and Barenblatt are suitable for polymers.
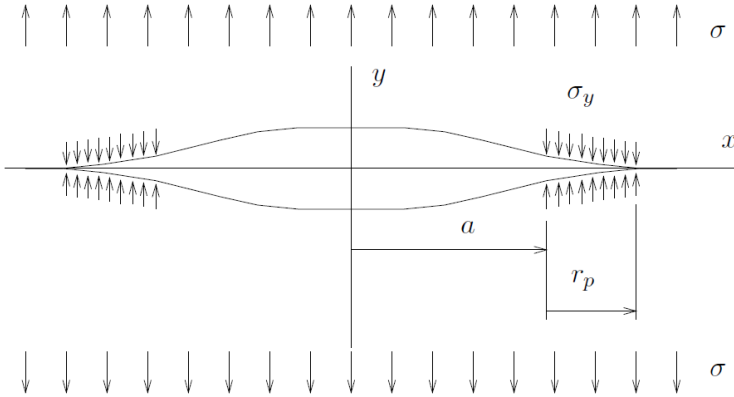
Figure 3.3: The plastic zone according to Dugdale-Barenblatt, [13].

3.3 Non Linear Fracture Mechanics- NLFM

If the plastic zone is too large or if the material is non-linear, LEFM is not applicable, neither the stress intensity factor. Non Linear Fracture Mechanics, NLFM, or Elasto-plastic Fracture Mechanics has to be used. Instead the crack tip opening displacement can be used in the crack growth criteria. The J-intergral method can also be used in NLFM. The J-integral describes the stress/displacement state in the crack tip zone, [13].

3.3.1 Crack tip opening displacement- CTOD

For LEFM the displacement in y-direction for a material point in the region around the crack tip can be calculated using distance and angle to the crack tip. For $\Theta = \pi$ a coordinate system with its origin in the center of the crack can be used to describe the displacement. The Crack Opening Displacement,COD, is two times this displacement and the Crack Tip Opening Displacement, CTOD, is zero. Replacing the crack length with effective crack length, and considering plasticity, the CTOD can be used in a crack criterion. In LEFM the CTOD can be related to G and K_I. In NLFM the CTOD is a measure of the deformation at the crack tip and can be compared to a critical value given by a crack growth criterion, [13]. The effective crack length can be expressed by using r_y from Irwin and adding the actual crack length. The crack tip opening can then be calculated. More about this can be found in [13]. Dugdales model can also be used for calculating the crack tip opening. The effective length is given by $a + r_p$. The crack tip opening displacement can be calculated and is not zero, [13].

3.3.2 J-integral

In NLFM, crack behavior can be analysed with the J-integral, introduced by Rice in 1968. It can replace the energy release rate in LEFM, [13]. It is a path independent contour integral with a value that is equal to the energy release rate in a nonlinear elastic body that contains cracks. Later it was showed that the crack tip stresses and strains in a nonlinear body can be uniquely described by J, [15]. The J-integral is the component in the x_1 - direction of the vector $\vec{J}$. It is given by integration along a trajectory Γ around the crack tip. From stresses and strains the specific elastic energy at each point of Γ is calculated. The integration can be chosen arbitrarily since it is path independent and the calculated values are compared to critical values measured according to normalized experiments.[13] More about the J-integral can be read in [22].

3.4 Failure of adhesive joints

When studying the failure of joints, in this case adhesive joints, the path for the crack propagation has to be considered. This results in the following three types of failure for adhesive joints. If the failure of the adhesive joint occurs in the interphase, or close to it, the failure is said to be adhesive. If the failure instead occurs in one of the substrate the failure is said to be cohesive. A mixture of these two is possible. By studying the location of the crack the weaknesses of the joint can be revealed. The different types of failure are shown in figure 3.4, [12].
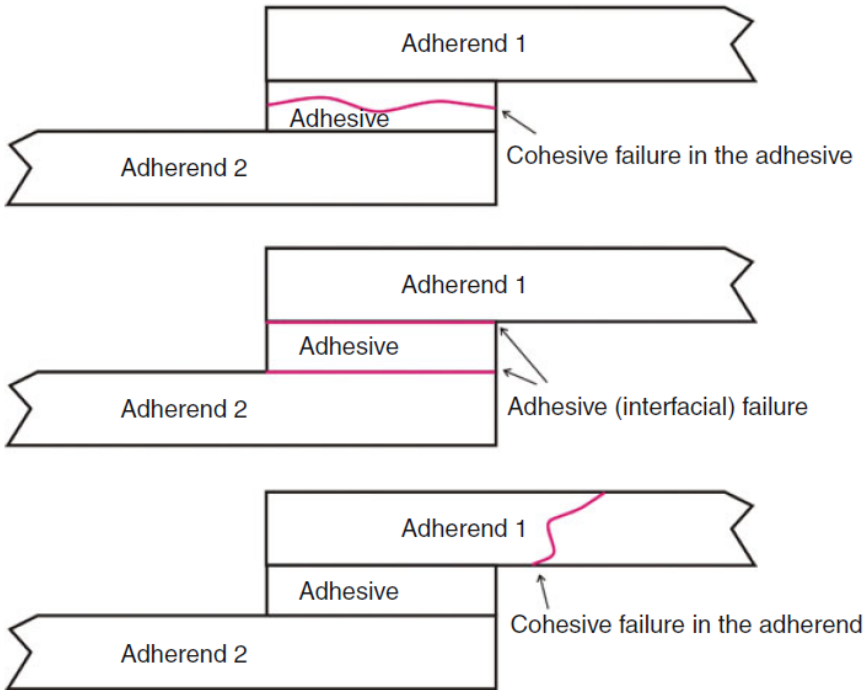
Figure 3.4: Failure types of adhesive joints, [3].

The capability of strain and toughness is much higher in compression and shear than in tension, cleavage or peel. Peel stresses occurs if one or both substrates are flexible, [6]. If the adhesive and adherends do not have the same thermo-mechanical properties internal residual stresses will be the result. These can cause failure without additional load being applied and they provide to the existing stresses at an interface, [7]. The surface structure affects the location of failure. When the surface is smooth failure occurs close or at the interface but for rough surfaces the failure is cohesive. The reason for cohesive failure is that yielding occurs at the fiber tips, moves in to the

polymer. The yielding gives rise to plastic deformations resulting in higher fracture energy than for the smooth surface, [4].

3.4.1 Fracture of heat seals

The plastic films can be sealed to package material using heat, so called heat seals. This can be done in a number of ways. There are three basic peel mechanisms for peelable heat seals.

- Adhesive peel

- Cohesive peel

- Delamination peel

For the adhesive peel, figure 3.5, the failure occurs along the interface between the layers sealed together. The strength of the adhesive peel is more sensitive to variation of sealing parameters then the other two peel mechanisms.
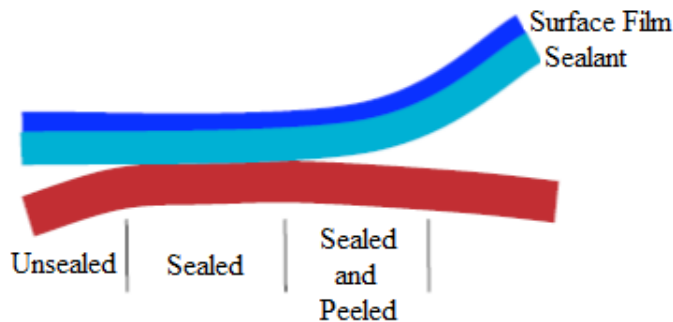
Figure 3.5: Adhesive peel, [16].

When peeled, thus when the surface film is pulled off, the sealant in a cohesive peel, see figure 3.6, splits. The seal strength is controlled by the amount of contaminants blended into the base resin. Cohesive peel sealants are more likely to string. Stringing is when the molecules stretch out across the gap that is created when separating the surfaces.
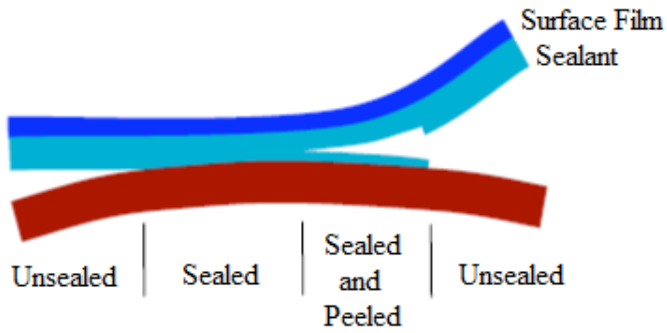
Figure 3.6: Cohesive peel, [16].

A delamination peel, also called interlaminar peel, delaminates when peeled, see figure 3.7. The peel has to be initiated by tearing or breaking through the sealant layer. Stringing are likely to occur for this type of peel, [16].
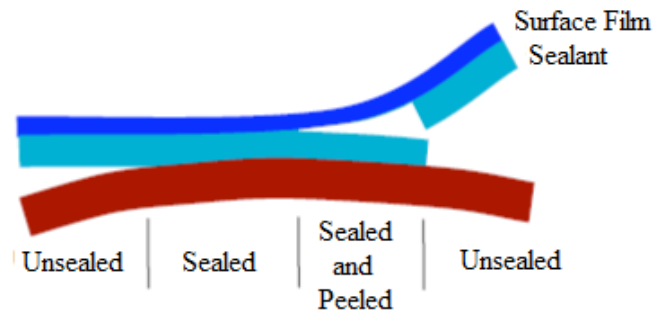
Figure 3.7: Delamination peel, [16].

Chapter 4

Packaging material

4.1 Material design

Packaging material consists of a number of material layers. Each layer contributes with desirable properties. A general structure of package material is shown in figure 4.1.
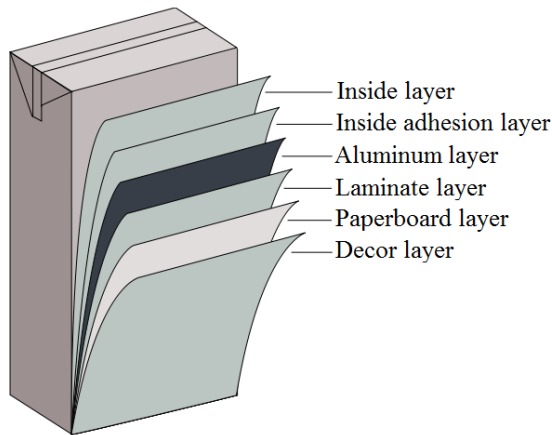
Figure 4.1: Generic package design.

The Decor layer is a polymer and is the external layer of the package, its role is to protect the paper and the print from damage and moist. The Paperboard layer is the load bearing material in the finished product and is considerably thicker than the other layers in the product. The Laminate layer is a polymer and its role in the product is to make the Aluminum layer

attach to the Paperboard layer. The Laminate layer is hard to separate from the Paperboard layer due to that the adhesion is stronger than the Paperboard layers internal strength. The Aluminum layers role is to block all light and to prevent diffusion. The Inside layer is a polymer. It holds the substance inside the finished product and make sure that the substance is protected from pollutions during its expected lifetime. The Inside layer must be resistant to the substance so that it does not dissolves and pollutes it. The Inside adhesion layer has stronger adhesion properties than the Inside layer and contributes to a stronger adhesion to the Aluminum layer. The Inside layer and the Inside adhesion layer is together called the Inside layer in the rest of the report.

4.2   Manufacturing

The process of combining the different layers into finished packaging material contains a lot of steps. The production rate is fast and the material is constantly moving. The result after one production cycle is a hundred meter long strip which is enough to produce thousands of containers. The strip is rolled to a massive coil with a diameter of up to 2 meter.
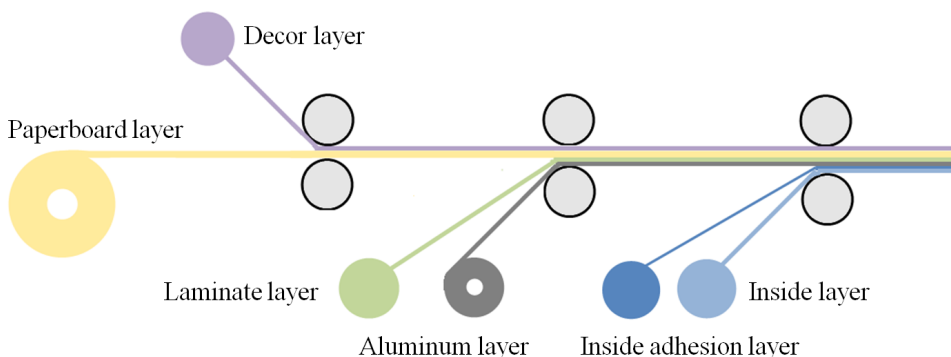
Figure 4.2: The manufacturing process.

To add an additional polymer layer during the manufacturing process a thin layer of the melted polymer is extruded on to the package material and rolled together. This leads to different properties in MD (machine direction) and CD (cross direction). The Paperboard layer and Aluminum layer that Tetra Pak uses is processed in a way that gives it different characteristics in MD and CD. The differences between the characteristics in MD and CD are often small for all layers except for the Paperboard layer. The direction out of plane is known as ZD (z direction), see figure 4.3.
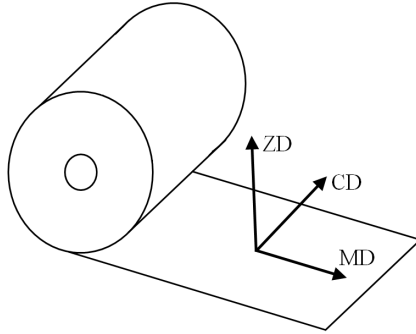
Figure 4.3: The material directions.

4.3 Test material

Three different materials have been analyzed to study how different thickness of the various layers in the packaging material affects the measured adhesion. The adhesions that this study focuses on is the one between the Inside layer and the Aluminum layer, further denoted as Adhesion 1, and the one between the Aluminum layer and the Laminate layer, further denoted as Adhesion 2, see figure 4.5. The different packaging materials are denoted as Material 1(M1), Material 2(M2) and Material 3(M3).

A rough sketch of the package materials is shown in figure 4.4. The combined thickness of the Aluminum layer and Inside layer is approximately 40 μm. The Paperboard layer is considerably thicker than the rest of the materials but is scaled down in the figure. M2 has a thinner Aluminum layer than M1 but they are otherwise identical. M3 has a thinner Inside layer than M2 and has half of the Laminate layer preattached to the Aluminum foil; otherwise they are identical. The materials are white, they have no print. This excludes the print as a variable parameter during the experimental tests.

All material is obtained after the manufacturing process so the material has not been exposed to any liquids or heating that occurs during the packaging process.

It is assumed that all layers except the Aluminum layer have the same properties regardless of which of the three package materials they are part of.

The surface properties of the Aluminum layer are important for Adhesion 1 and 2. The two surfaces of the Aluminum layer have different roughness. The surface towards Adhesion 1 is always the rougher one. This affects the interlocking properties of the adhesions, in general the adhesion strength increases with the roughness.
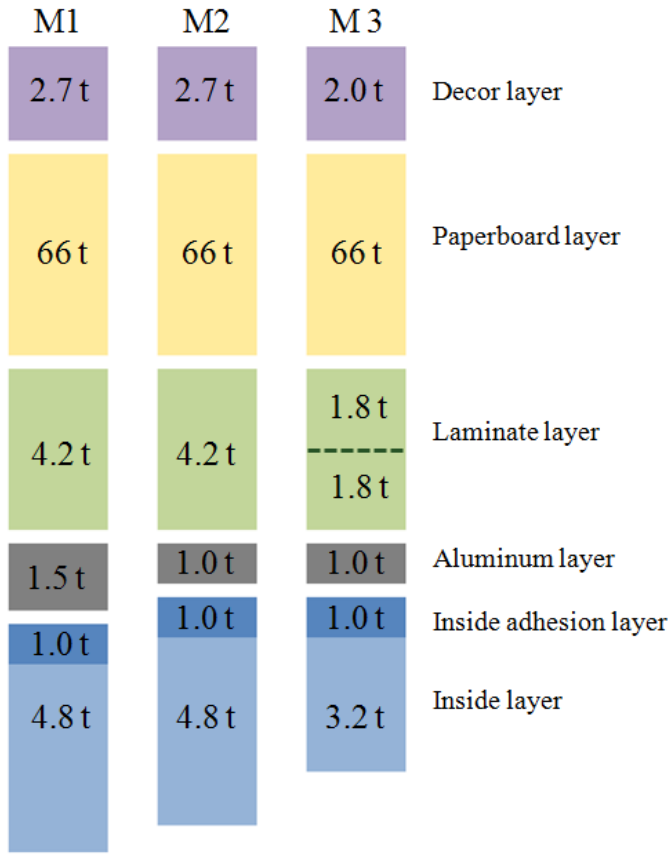
Figure 4.4: The Geometry of the materials.
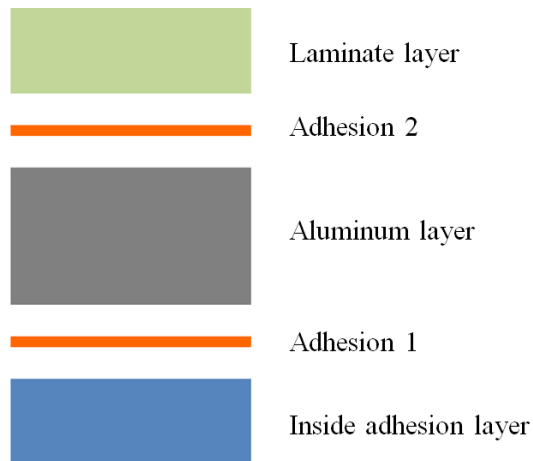
Figure 4.5: Definition of the adhesions.

Chapter 5

Adhesion tests

5.1 Standard tests

There are standard methods for measuring adhesion, these standard methods are very good in most cases but are difficult to use when the dimensions of the test specimen are too small. Most tests are made to test an adherend that can be applied between two surfaces which makes the wanted test setup easy to obtain.

The tests shown in figure 5.1 are very hard to perform on packaging material since the dimensions are very small and the stiffnesses are low. Moreover the adhesion surface cannot properly be recreated in a test rig since it is impossible to include the effects of the high speed during the manufacturing of the package material. If one of the tests in figure 5.1 would be used on the packaging material the paperboard would delaminate before the adhesion would break since the paperboard has a very weak mid-layer.
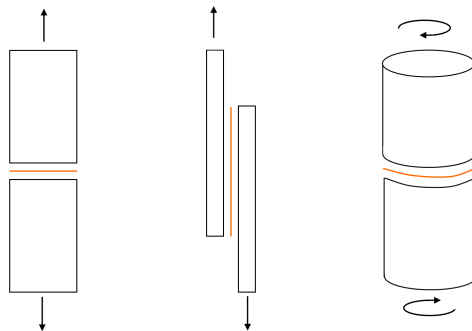
Figure 5.1: Standard tests.

Tests suitable for thin layers are show in figure 5.2. The most suited tests when one part is thin are peel tests. The basic principle of a peel test is that the thin part, the peel arm, is pulled off from a much stiffer surface.
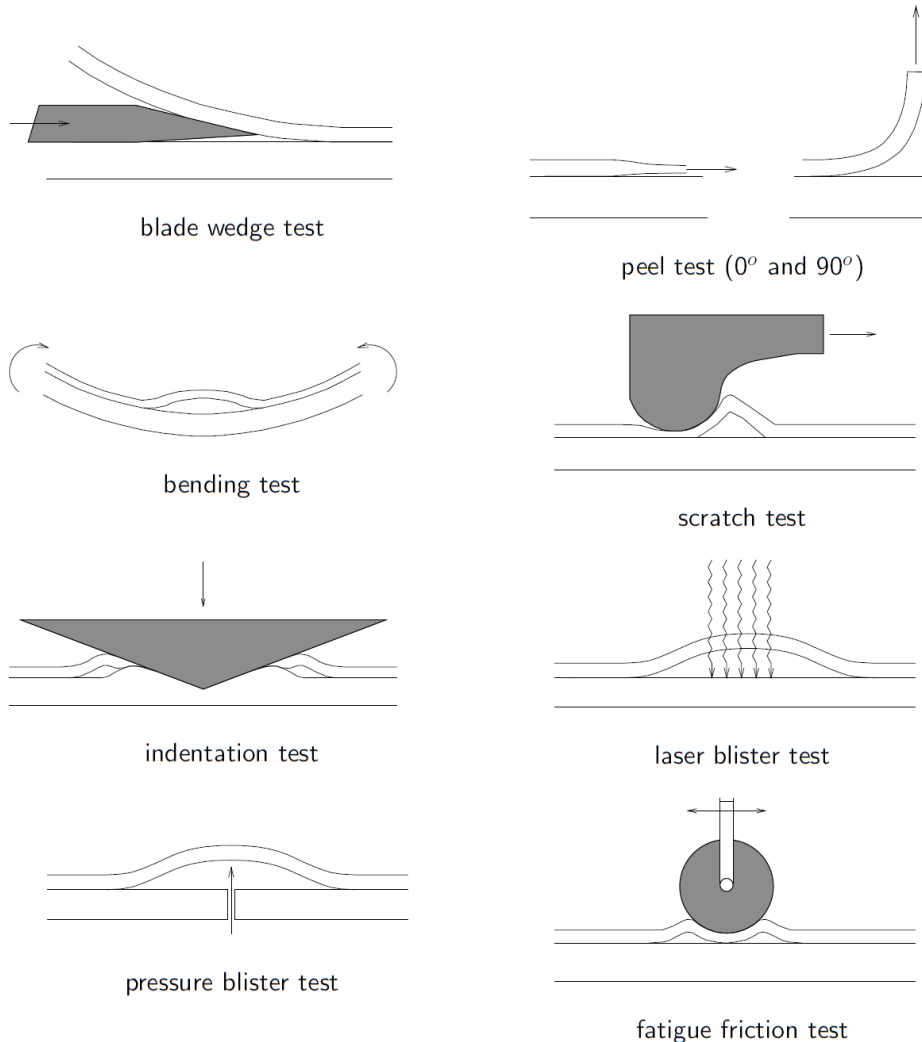
Figure 5.2: Adhesion tests for thin layers, [13].

5.2 Peel test

Peel tests are the most used type of tests for determining adhesion for thin ductile materials because the tests are fast and easy to make and the test rig is simple. The theory behind peel tests are easily derived when the simplifications that the peel arm is infinitely stiff when pulled and totally flexible

in bending are made, the total energy to separate the surfaces for these assumptions is known as $G^{\infty E}$. To calculate the energy required for separation, the parameters shown in figure 5.3 must be known.
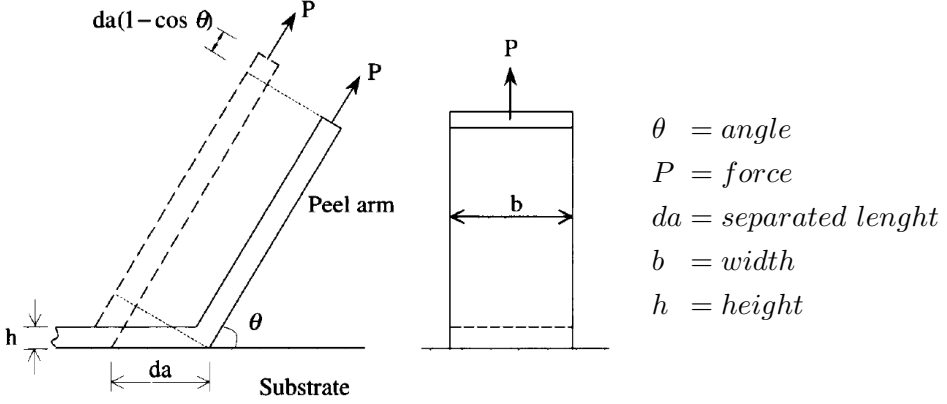
Figure 5.3: Peel test, [10].

The energy is given by the work done by the force. The distance of the force is $da(1 - \cos\theta)$ which gives the energy $P \cdot da(1 - \cos\theta)$ that is required to separate the area $b \cdot da$, [10].

$$G^{\infty E} = P \cdot \frac{da(1 - \cos\theta)}{b \cdot da} = \frac{P}{b}(1 - \cos\theta) \tag{5.1}$$

This is a very simplified model but it is the basic concept for the peel tests. Effects that come into account when a more advanced models is used are elongation of the peeling arm, bending and plasticity in the peel front, kinetic energy and root rotation (the angle in the peel front), [10].

The fracture energy for non simplified system can be described as:

$$G_C = \frac{dU_{ext} - dU_s - dU_d - dU_k}{b \cdot da} \tag{5.2}$$

$dU_{ext} = external\ input\ energy$

$dU_s\ \ = energy\ stored\ in\ strain$

$dU_d\ \ = dissipated\ energy$

$dU_k\ \ = kinetic\ energy$

5.3 Peel arm

The peel arm is hard to describe mathematically if it plasticize and its width shrinks, also known as necking. Plastic deformation leads to a nonlinear stress-strain curve for the peel arm and energy will be dissipated into plastic deformations. The elongation of the peel arm due to loading is described as ϵ and this will increase the energy inserted into the system, [10].

$$\frac{dU_{ext}}{b \cdot da} = \frac{P}{d}(1 + \epsilon - \cos\theta) \tag{5.3}$$

The strain of the peel arm will also affect dU_s and dU_d. It is not important to separate these two components.

$$\frac{d}{b \cdot da}(U_s + U_d) = h \int_0^\epsilon \sigma d\epsilon \tag{5.4}$$

Eq. 5.3 and 5.4 combined with eq. 5.2 yields

$$G_c^{eb} = \frac{P}{b}\left(1 - \cos\theta + \frac{1}{\sigma}\int_0^\epsilon \sigma d\epsilon\right) \tag{5.5}$$

When the stress is proportional to the strain to the power of n, $\sigma \propto \epsilon^n$, then the last part can be rewritten.

$$\frac{1}{\sigma}\int_0^\epsilon \sigma d\epsilon = \frac{n}{1 + n} \cdot \epsilon \tag{5.6}$$

5.4 Kinetic energy

The kinetic energy in peel tests are often negligible due to the low mass and low speed of the peel arm. $E = \frac{1}{2}mv^2$ is used when deriving the kinetic energy, [10].

$$\frac{dU_k}{b \cdot da} = \frac{1}{2}\rho h v^2((1 - \cos\theta)^2 + \sin^2\theta) = \rho h v^2(1 - \cos\theta) \qquad (5.7)$$

$$
\begin{aligned}
\rho & = density\ of\ the\ peel\ arm \\
v & = speed\ of\ the\ peeling \\
1 - \cos\theta & = horizontal\ speed\ component \\
\sin\theta & = vertical\ speed\ component
\end{aligned}
$$

The kinematic energy, eq. 5.7, can be included in both eq. 5.1 and 5.5.

5.5 Plasticity in release joint

If $\theta \neq 0$ then there will be moment forces in the peel front due to eccentricity of the applied force. The moment will cause elastic deformation and in some cases also plastic deformation in the peel front. The elastic energy will return to the system when the section is moved away from the peel front. The energy dissipated into the plastic deformation is lost, [10].
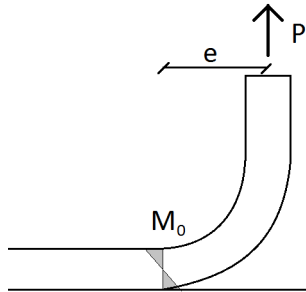
Figure 5.4: Eccentricity in the peel front.

5.6 ICPeel

Imperial College, London, has made two excel documents called IC Peel (2006) and IC Peel (Digitised) 07, [17]. These excel documents calculates the theoretical adhesive strength from a small number of parameters of a peel test. The drawback of the IC Peel programs is that the theory behind them is hard to understand in a short amount of time.

The adhesion properties from the IC Peel programs correspond badly with what commercial finite element programs uses to get the same resulting force

as from the experimental tests. Except from uncertainties in the ABAQUS model, a difference when comparing results for Adhesion 1 could depend on the vague assumption that IC Peel uses Euler-Bernoulli beam theory. This is far to simple for describing the complex deformations in the peel front due too the small geometry and soft nature of the Inside layer. Adhesion 2 has two layers in the peel arm which is something that ICPeel sheets does not have an option for.

Assume that Adhesion 1 is the same for all materials and that IC Peel yields the right result for 90°, M1 and the force of 5.95. If the same value for G_C and σ_{max} is used but the thickness of M2 is inserted into IC Peel 2006 then a seperation force of 5.39 N is needed but the result from the experimental tests is 4.64 N.

5.7 Further reading

For further readings about the theory of peel arm mechanics, see [10].

Chapter 6

Experimental tests

Experimental tests were performed at Material analysis laboratory at Tetra Pak in Lund. The primary aim was to gather experimental test results for Adhesion 1 and Adhesion 2 and to better understand the mechanisms and phenomenon involved when breaking adhesion in a package material. Another aim was to document the mechanical behaviour so comparisons and input to FE-models could be made. Photos were taken and videos were recorded to capture the deformations during the tests.

6.1 Performed tests

The chosen tests were 0°, 90° and 180° peel tests, the peel fronts are shown in figure 6.1. Adhesion 1 and Adhesion 2 were tested in these three angles. It is important to test more than one angle for each adhesion if comparisons are to be made with simulations. The reason for not performing tests for more angles were that time and equipment were limited. The peel test in 0° is especially interesting since it mainly tests the shear behaviour of the adhesion strength which is the most common type of adhesive failure in packaging materials. M1, M2 and M3 were tested with specimens taken in the MD; M2 was in addition tested in CD to see if there was any difference.

6.2 Test design

6.2.1 Specimen preparations

The packaging material was placed in the laboratory, to be conditioned, at least 24 hours before the tests were performed. The climate in the laboratory
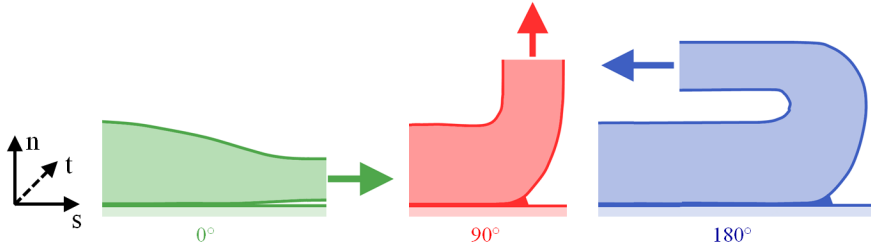
Figure 6.1: Chosen peel angles.

was controlled to 23°C and 50 % humidity. Specimens were taken from the whole width of the packaging material to investigate the influence of the location along the width. The specimens were cut into 15 mm wide stripes and from package material without print.
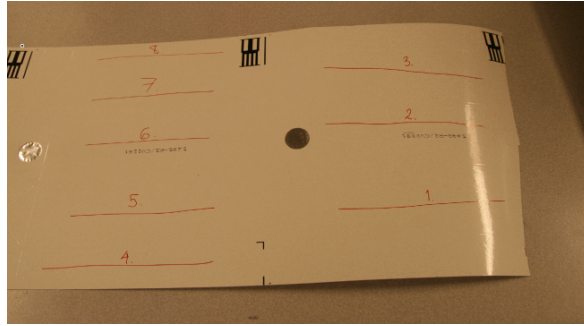
Figure 6.2: Packaging material with marked specimens in MD-direction.

For Adhesion 1 the Inside layer was carefully peeled off by hand to create a peel arm. The Inside layer was peeled off in an angle of 180°, which led to the peel arm being plasticized prior to the test. When the peel arm was long enough to be mounted properly in the test machine the stripe was cut into a length of around 50 mm. The Inside layer was gently cut 20 mm from the peel front, with the aim of not cutting into the Aluminum layer. The distance that were peeled off was then approximately 20 mm with a total area to be peeled of approximately 300 mm^2. This was done to determine the total amount of energy required to separate a known area. For the 90° test a double sided tape was pasted onto the Decor layer before the stripes were cut out to attach the specimen to the test wheel, see figure 6.5. A prepared specimen for Adhesion 1 is shown in figure 6.3.

For Adhesion 2, 0° and 180°, the Inside layer and Aluminum layer were peeled off and folded in 180° before stripes were cut out. The Aluminum layer was placed downwards when cut. The stripes were cut into lengths of ca 50 mm.

38

Also the Adhesion 2 specimens were cut 20 mm from the peel front. Both the Inside layer and the Aluminum layer were cut in this case. For the 90° test a double sided tape was pasted onto the Decor layer of the material after the Inside layer and the Aluminum layer was peeled off to attach the specimen to the test wheel, see figure 6.5. A prepared specimen for Adhesion 2 is shown in figure 6.4.
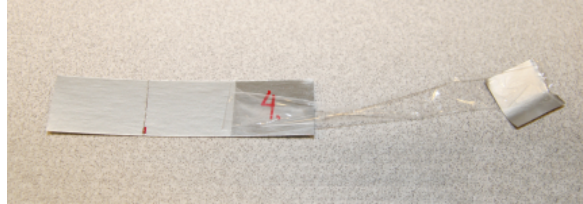
Figure 6.3: Adhesion 1 specimen, separation of Inside layer to the Aluminum layer.

Figure 6.4: Adhesion 2 specimen, separation of the Inside layer and Aluminum layer to the Laminate layer.

6.2.2 Machine settings

All peel tests were performed in an Instron machine, which is displacement controlled. The force with which the peel arm was pulled and the displacement of the upper clamp were registered.

For the 0° and 180° tests the specimen was mounted in the lower clamp of the machine before the peel arm was mounted in the upper clamp. When performing the 90° tests the lower clamp was substituted with a frictionless wheel. The specimens were attached with tape to the wheel before the peel arm was mounted in the upper clamp. The distance between the lower clamp/the wheel and the upper clamp was approximately 50 mm for all tests. The initial lengths of the peel arms before the tests started were not measured. This length affects the angle of the force-displacement curve before the plateau force is reached, see figure 6.6. The rate of the upper clamp, the

pulling device, was 50 mm/min for 0° and 90° and 100 mm/min for 180°. The difference in pulling rate was introduced so that the rate of which the peel front opened should be approximately the same in all tests. When Adhesion 1 was tested the peel arm extended differently in the different angles due to that the peel force differs. To get similar crack propagation rate in the peel front, the extension of the peel arm should be taken into consideration when determining the applied displacement rate. This was not considered in these tests but is not hard to implement in future projects.
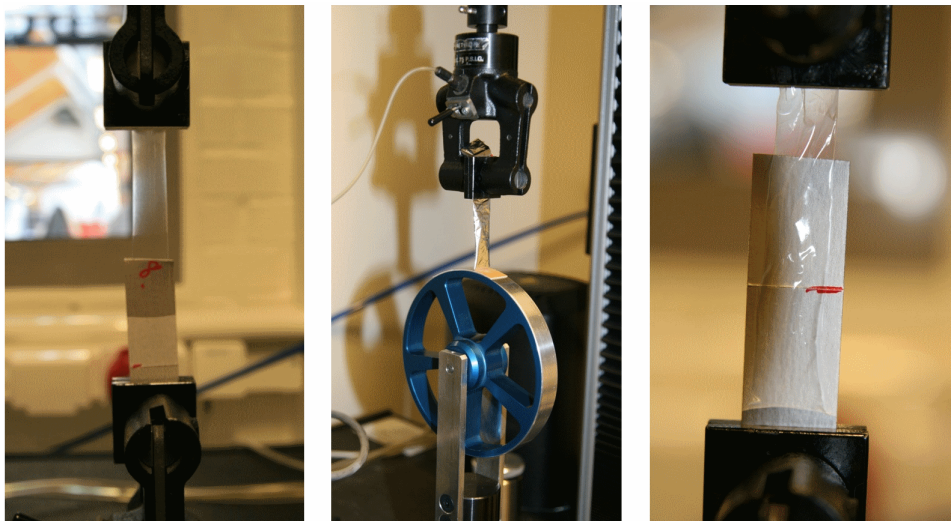
Figure 6.5: Experimental test setup, left: 180°, 100 mm/min, center: 90°, 50 mm/min, right: 0°, 50 mm/min.

6.3 Results

The tests were performed until 10 representative curves for each test angle were obtained. This applied to both Adhesion 1 and Adhesion 2. Curves for specimens that for example delaminated or where the Aluminum layer cracked were deleted and not taken into account since the adhesion was not measured correctly for these cases. For Adhesion 2, 180° the number of presented curves are only 5, for reasons given in 6.3.2. A sketch of a curve is shown in figure 6.6 and the results from the experimental tests are found in table 6.1 and table 6.2. All result graphs can be found in Appendix A. The values in table 6.1 and table 6.2 are mean values.

For each single specimen of all packaging materials and all angles a mean value of the plateau peel force was calculated. Then a final mean value was calculated from the 10 specimen mean values of every test setup, these are
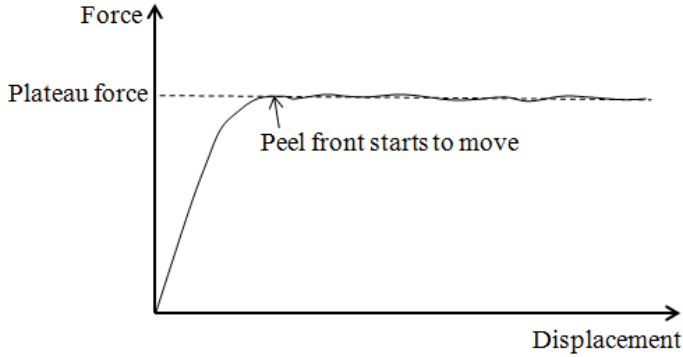
Figure 6.6: Sketch over force-displacement curve.

shown in table 6.1 and table 6.2. The standard deviation was calculated using the specimen mean values of the peel force. The results were assumed to be normal distributed and a 95 % confidence interval was calculated. The confidence intervals are presented in the graphs in Appendix A together with each test result and the mean curve. The standard deviations are found in table 6.1 and table 6.2.

Test results MD						
Adhesion 1	0°	std	90°	std	180°	std
M 1	7.29	0.180	5.95	0.145	5.49	0.096
M 2	7.06	0.139	6.05	0.150	5.38	0.095
M 3	5.52	0.164	4.64	0.084	4.25	0.108
Adhesion 2	0°	std	90°	std	180°	std
M 1	–	–	1.38	0.022	1.18	0.031
M 2	–	–	1.38	0.084	1.18	0.057
M 3	–	–	1.45	0.043	1.24	0.107

Table 6.1: Test results for Adhesion 1 and Adhesion 2 with standard deviations.

Test results CD						
Adhesion 1	0°	std	90°	std	180°	std
M 2	6.55	0.158	5.86	0.158	5.18	0.111
Adhesion 2	0°	std	90°	std	180°	std
M 2	–	–	1.32	0.042	1.06	0.034

Table 6.2: Test results for Adhesion 1 and Adhesion 2 with standard deviations.

6.3.1 Adhesion 1
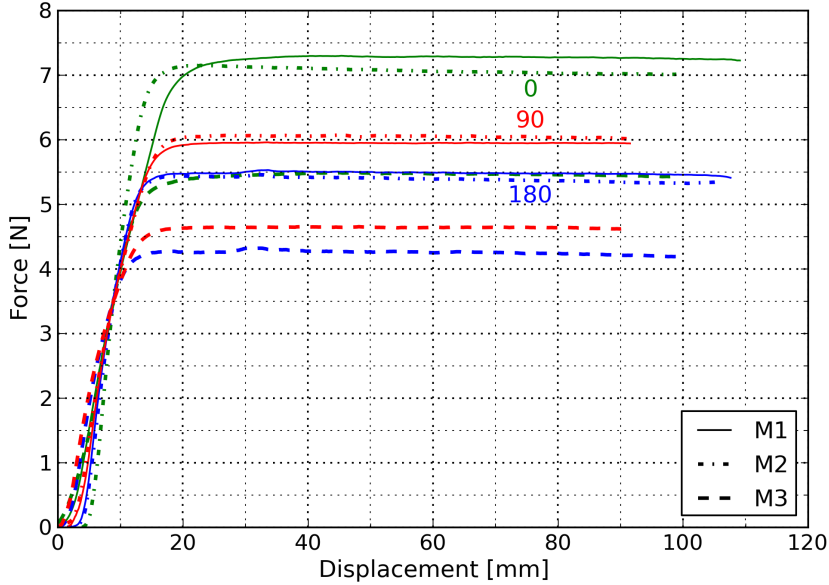
Figure 6.7: Mean curves for Adhesion 1.

A few more than 10 specimens had to be tested to get 10 representative curves for all angles and for all materials. Except for M3 in 90° for which the specimens delaminated between the two polymers of the Inside layer approximately every second specimen. Over all, the specimens of M3 were harder to prepare since the Inside layer broke more easily when peeling off the peel arm.

The standard deviation is quite small for all materials and all angles. This indicates that the tests are insensitive to small differences in specimen preparation and machine mounting. It also indicates that the adhesion is consistent over the width of the packaging material roll. M3 shows the widest range regarding total displacement in 0° and 180°. M1 and M2 seems to result in approximately the same displacement.

It is evident from figure 6.7 that the plateau force for M1 and M2 are very close to each other for all angles. M3 has for all angles a plateau force lower than the two other materials. It is also evident that the peel force decreases when the peel angle increases, the peel force is lowest for 180° and highest for 0°.

Looking at the results from testing the materials in the CD it is clear that

the peel force differs between MD and CD. The peel force is higher in MD than in CD for all package materials and all angles.

The peel front and the deformation of the peel arm are shown in figure 6.9. The width of the peel arm decreases during the first centimeters to then stabilize. It was noticed that if the peel arm was extended and then stopped, the peel front continued to propagate for 1-2 seconds.
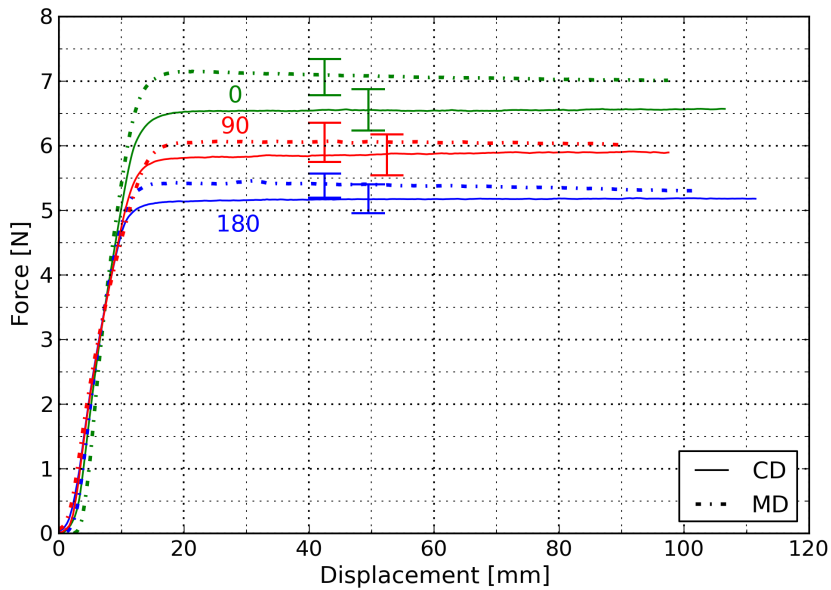
Figure 6.8: Adhesion 1, M2, MD vs CD.
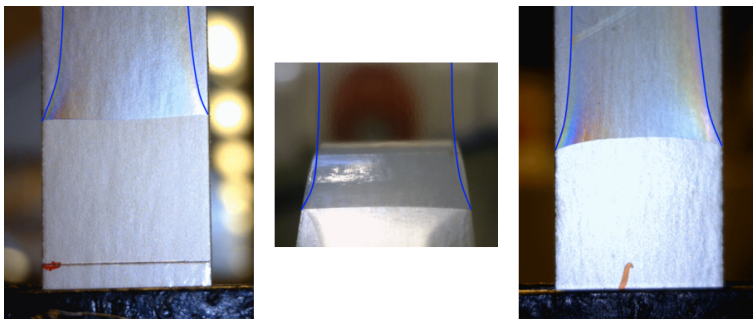
Figure 6.9: Adhesion 1, left: M2 0°, center: M1 90°, right: M3 180°.

43
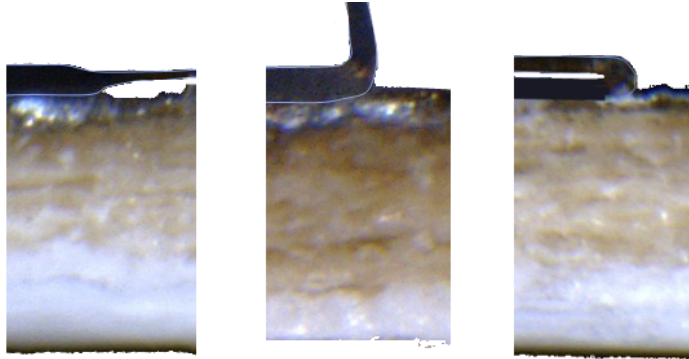
Figure 6.10: Peel front Adhesion 1, left: M2 0°, center: M1 90°, right: M3 180°.

6.3.2 Adhesion 2
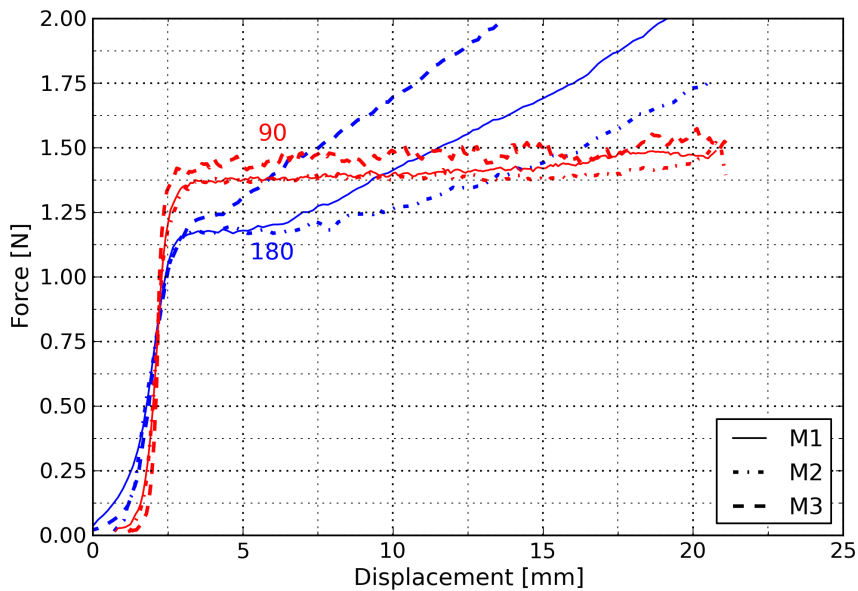
Figure 6.11: Mean curves for Adhesion 2.

The 0° test for Adhesion 2 was not possible to perform because the Aluminum layer broke before the adhesion separated due to the force becoming to large. For 180° it was hard to obtain results showing a plateau value, expecially for M3, due to that the Aluminium layer was breaking at the edges causing a damage which propagated. For M3 it was difficult to obtain satisfying results for the 90° test for the same reason. The peel forces for M1 and M2 were

similar; this applies to both tested angles. For M3, however, a higher peel force was reached for both angles. See figure 6.11.

The graphs are more fluctuating for Adhesion 2 than they are for Adhesion 1, see Appendix A. Higher peaks can be observed in most of the tests. Even though the graphs are fluctuating the standard deviations are small.

For Adhesion 2, the peel arm is stiff and therefore its deformation can be neglected. No necking of the peel arm at the peel front was observed, see figure 6.13.

In CD the peel force was lower than in MD, this applies to both angles.
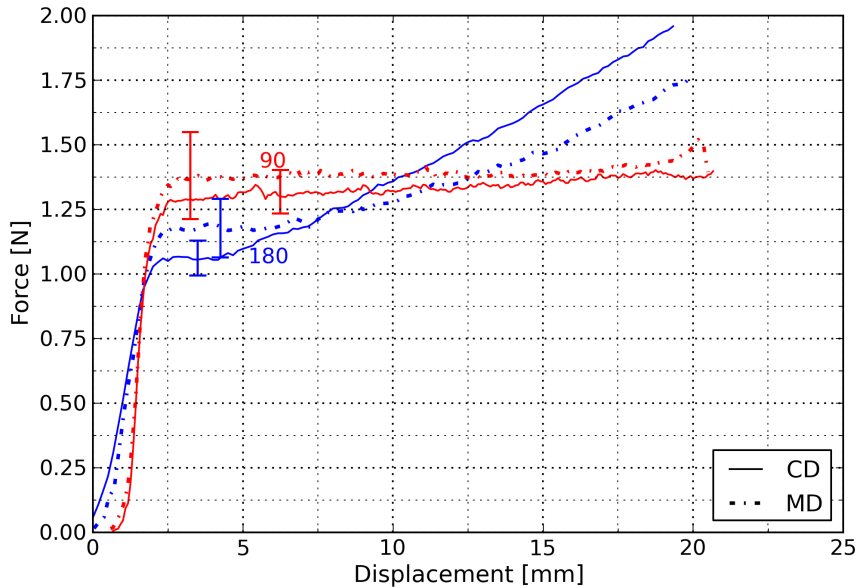
Figure 6.12: Adhesion 2, M2, MD vs CD.
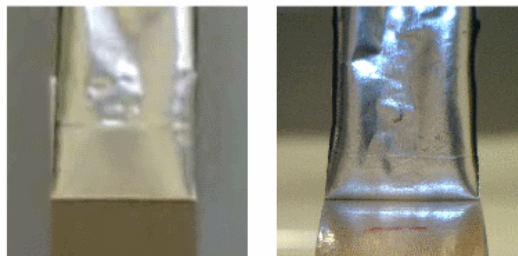
Figure 6.13: Adhesion 2, left: M3 180°, right: M1 90°.

6.4 Discussion

6.4.1 Adhesion 1

The result that the peel force was the same for M1 and M2 indicates that the adhesion is the same for these two materials, since they have the same thickness of the Inside layer and approximately the same displacement was measured. That lower force of Material 3 seems reasonable since the Inside layer is thinner and the force needed to plasticize the peel arm is lower.

The reason for the wider range in total displacement for material 3 could be that flaws in the material affects the extension more in a thinner peel arm. Another reason for the distribution in total displacement is probably caused by the fact that the distance, 20 mm, from the peel front to the cut was not exact since it was measured with a ruler and cut by hand.

The reason for that the force needed to break the adhesion was decreasing with a decrease in angle could be due to that the area that transfers the stresses between the material layers increases with decreasing angle.

The small peaks at approximately 30 mm for 180°, see figure A.13, could possibly be explained by a disturbance of the machine in some way.

The stiffness was found to be higher for M2 in 0° than that of the other two materials which may be be explained by the fact that the upper clamp possibly was placed closer to the lower clamp than during the other tests.

The Aluminum layer is rolled during the manufacturing process that gives different properties in MD and CD. This together with that the polymer molecules align during the manufacturing process could explain the difference in the plateau force for MD and CD. To explain why one is higher than the other more detailed information about the surfaces has to be known.

The low stiffness of the Inside layer causes the deformation in the peel arm close to the peel front. The deformation triggers traction concentrations at the edges.

The results from the Adhesion 1 tests indicate that the adhesion is the same for M1, M2 and M3.

When 90° was tested, the Paperboard layer delaminated locally under the peel front as it propagated, and the tape under the peel front was stretched in the thickness direction.

For Adhesion 1 necking was observed which affects the stress distribution on the edges that can lower the peel force.

6.4.2 Adhesion 2

The peel force was very similar between M1 and M2; this result is hard to interpret since the Aluminum layer for M1 is thicker and has different properties.

Preparations of specimens of M3 were in general tricky. The Aluminum layer was hard to remove. This could be because the strength of the adhesion was more uneven over the surface since it had a pre laminated polymer layer.

The fluctuating values that are observed in most of the graphs could be because the edges of the Aluminium layer is more affected by the cutting process than the Inside layer is for Adhesion 1. The higher peaks are due to that small cracks at the edges are developed in the Aluminum layer, that dissipates energy. The peaks in force just before the end of the tests are because the Paperboard layer delaminates, this is due to that the cut at 20 mm is too deep and it has damaged the outer layer of the Paperboard.

The result that the standard deviations are small even though the graphs are fluctuating is because the mean values of the test specimens lies close to each other.

The result indicates that Adhesion 2 is not the same for the M1, M2 and M3. M3 has a thin pre attached Laminate layer and this could cause the difference in peel force.

Since the Aluminum layer and the polymer have different properties in MD and CD, it could explain the difference in the plateau force for MD and CD. To explain why one is higher than the other more detailed information about the surfaces has to be known.

6.4.3 Evaluation of test method

Peel tests are easy and fast to prepare and they are not sensitive to minor differences in preparation and mounting. The standard deviations are small which indicates that the result is reliable. It is beneficial that three angles can be tested in the same machine. With new fasteners more angles can be tested.

It is hard to evaluate a single property from a peel test since many variables affects the result. The stress distribution in the peel front is complex which

makes it hard to evaluate adhesive properties, i.e. σ_{max} or the traction separation behaviour in the different directions. It was not possible to determine the release distance from the photos taken during the tests. The energy which is required to separate the surfaces is hard to evaluate since some of the energy goes to viscoelastic effects, plastic and elastic strain of the whole peel arm and plastic bending deformations in the peel front.

As mention before, pure tests of the adhesion in normal direction and shear direction, respectively, would be preferred.

Chapter 7

Material models

This chapter describes the different material models used in the simulations described in chapter 8. The material models have been based on samples that are as similar as possible to the material layers in M1, M2 and M3. It is cumbersome to obtain undeformed specimen of the different layers to study if it is not done during the manufacturing process.

7.1 Inside layer

The material model for the Inside layer has been taken from [18], it is not the same material as the Inside layer but was considered to be close enough. The reason for not testing the actual Inside layers of M1, M2 and M3 was because it was not possible to get underformed specimens of the layers during the manufacturing process of the package material. Two different sets of material properties have been used for the Inside layer. One with the correct initial Young's modulus and one with Young's modulus set ten times higher, both yields similar response curves. The one with the correct initial value behaves better for small deformations due to that the relationship between plastic and elastic strain is correct. The one with ten times higher Young's modulus behaves better for large deformations due to that the stiffness of the Inside layer increases with the strain. The response curve can be seen in figure 7.1.

When simulating Adhesion 1 the higher Young's modulus is used due to that large strains occurs. When simulating Adhesion 2 the initial value for Young's modulus is used due to that the Aluminum layer prevents large deformations of the peel arm. Isotropic hardening is used, see section 7.4.
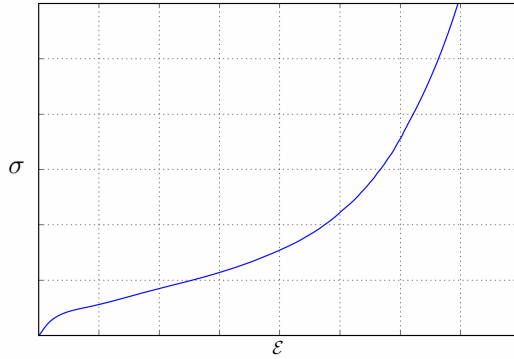
Figure 7.1: Response curve, Inside layer.

7.2   Aluminum layer

The material properties for the Aluminum layer has been taken from tensile tests, the manufacturer is unknown.

The thickness affects the properties of the aluminum foil. The response curve for the thinner aluminum layer used in all simulations is shown in figure 7.2. The thicker foil has a higher Young's modulus and higher yield point but the point of failure is approximate at the same stress and strain as for the thinner foil. The properties for the thicker aluminum foil is never used in the simulations. The lower stress-strain relationship for the thinner foil could be explained by that its thickness is less than the normal size of aluminum crystals. Isotropic hardening is used, see section 7.4.
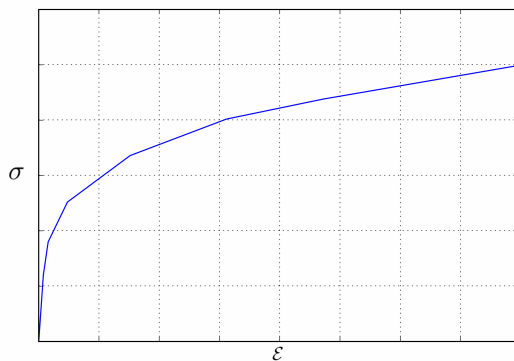
Figure 7.2: Response curve, Aluminum layer.

7.3 Paperboard-, Laminate- and Decor layer

The Paperboard- , Laminate- and Decor layer were considered as a rigid base. This is not true but it was done to reduce the number of input parameters. To capture the delamination behavior of the Paperboard layer is difficult and it is not the focus of this study.

7.4 Material hardening models

The material will be subjected to cyclic loading and it is therefore important that the hardening of the material is correct. The three most common models are isotropic hardening, kinematic hardening and combined hardening.
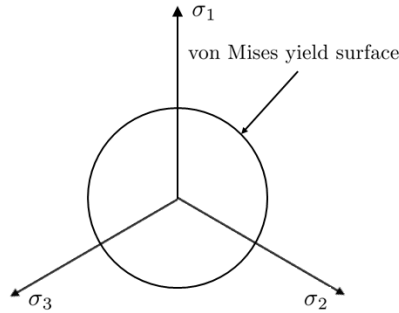
Figure 7.3: von Mises yield surface in the deviatoric plane.

7.4.1 Isotropic hardening

Isotropic hardening makes the material stiffer in all directions while it maintains its place in the deviatoric plane, it is shown in figure 7.4. This means that if a material is subjected to a compressive force its σ_{yield} for a tensile force is increased with the same amount, [21].

7.4.2 Kinematic hardening

Kinematic hardening does not make the material stiffer in other directions when hardened, it is shown in figure 7.5. This means that the response curve will join the unhardened curve for tensile after being subjected by compression, [21].

7.4.3 Combined hardening

Combined hardening is a mix between isotropic and kinematic hardening, it is shown in figure 7.6. Combined hardening is usually the most correct model but the mixture between isotropic and kinematic hardening should first be known. Just guessing would probably yield a more accurate result in the simulations but to keep the unknown parameters to a minimum this option is not chosen, [21].

7.5 Adhesive layer

7.5.1 Simulating adhesion numerically

There are a number of ways to treat crack propagation and adhesion in ABAQUS. When interested of simulating failure of an adhesive bond or crack propagation along an interface, when the crack propagation path is not arbitrary, cohesive elements and cohesive surfaces are relevant. When simulating delamination numerically; two types of approaches can be used, direct application of Fracture mechanics or the framework of Damage mechanics, [14]. The cohesive behavior, which has been implemented in the simulations, is counted to the Damage mechanics approach.

Damage Mechanics

Damage mechanics are based on the cohesive crack model developed by Dugdale. It states that the stress is limited to the yield stress and that the plastic zone in front of the crack tip is strip-shaped, see 3.2.3. Barenblatt and Hilleborg developed the model so that it holds on molecular level and so that it allows for existing cracks to extend and new to develop. Cohesive zone models are more powerful than Fracture mechanics since they predict both damage initiation and damage. Tractions and separations at the interface are related in the damage zone model by a constitutive equation. The constitutive equation can be determined using either a mechanistic approach, in which for example the J-integral can be used, or by using results from experimental tests, which are compared to results given by prediction models. One alternative is to use a predefined softening curve that are fitted to the experimental findings; another is to use characteristic points of the traction-separation curve. The simplest is to use a bilinear constitutive equation, see figure 7.7. When the maximum traction is reached damage is initiated and when the area under the traction-separation curve equals G_c the crack propagates. If pure loading in either normal or one of the shear directions is the case then the traction strength and G_c in that direction determines the
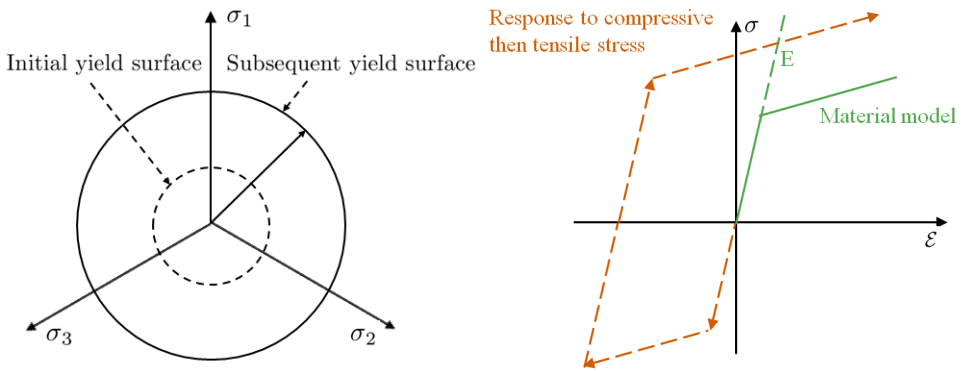
Figure 7.4: Isotropic hardening.
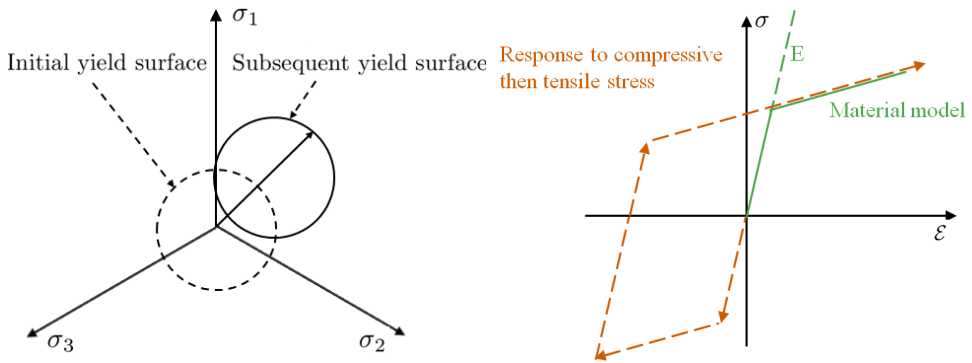
Figure 7.5: Kinematic hardeing.
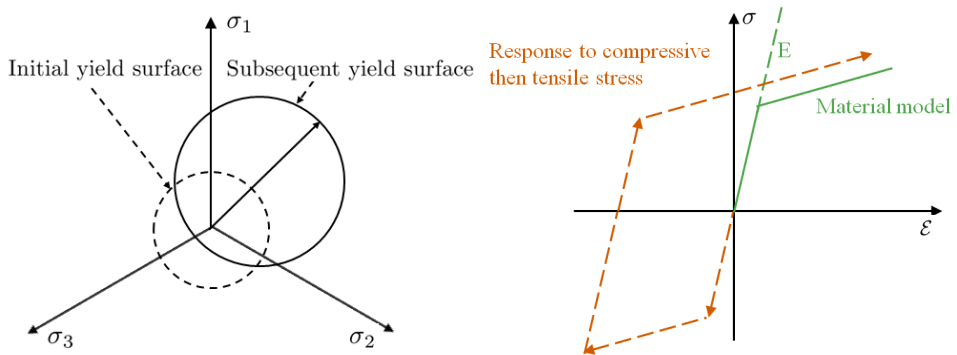
Figure 7.6: Combined hardening.

traction-separation curve. If the load case is a mix of the modes coupling effects between the modes must be taken into account. Damage initiation occurs when

$$f_{initiation} = f(\tau_i) - 1 = 0 \tag{7.1}$$

Were $f_{initiation}$ is the initiation criterion and $f(\tau_i)$ is the norm of the tractions.

The damage propagation criteria is described independent of the initiation.

$$f_{propagation} = f(G_i) - 1 = 0 \tag{7.2}$$

$f_{propagation}$ is a function of the pure mode energies and $f(G_i)$ is a norm of the energy release rates.

The traction-separation relation has to be modified when implemented numerically. An elastic path is introduced to be able to implement the cohesive zone in ABAQUS. If the stiffness is chosen too high convergence problems may occur.

(a) Physical model   (b) Numerical model
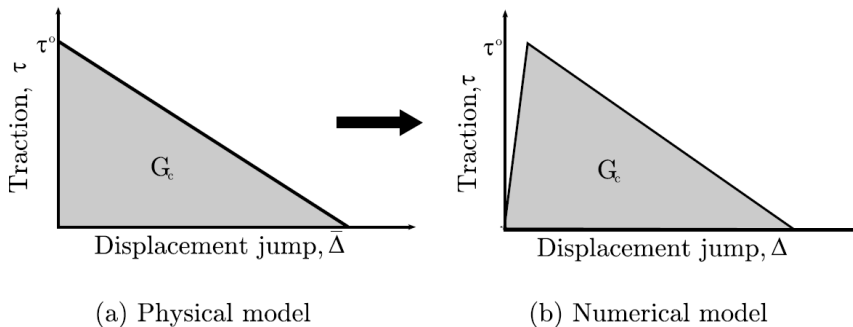
Figure 7.7: Traction-displacement curves [14].

There are two ways to implement the cohesive zone model into a simulation. The first is based on discrete interelement cracks and are in ABAQUS called cohesive elements. The crack extends between elements and are often used when simulating delamination of multilayered materials. In the simulations of this report the crack path is known but if this was not the case remeshing would have to be done as the crack extended, [14]. For cohesive elements damage is a material property,[19]. The second is based on intraelement approach. Extra sets of degrees of freedom are added to the mesh and these determines the magnitude of displacement field jump that is the result of

the crack. This can be done since a discontinuous mode can be allowed due to the introduction of strong discontinuity kinematics in the continuum medium. This introduction gives that specific traction-displacement laws are fulfilled at a discrete set of propagating cohesive surfaces. The need for extra degrees of freedoms make this strategy harder to implement, [14]. For cohesive surface behavior damage is an interaction property, [19]. There are many simularities between using cohesive elements and using cohesive surfaces. The adhesive layer was simulated using cohesive elements. Cohesive elements were chosen because it is visually easier to evaluate the stresses and shape of the peel front and because cohesive elements can have a denser mesh than the surroundings. There are three different models for defining the mechanical constitutive behavior for a cohesive element; traction-separation, which was used in the simulations, continuum and gasket. (Analysis users manual 32.5.1)

7.5.2 Cohesive elements

Traction- separation law and damage initiation

The traction-separation behavior prior to damage initiation and damage evolution is linear elastic. The elastic behavior is given, in three dimensions, by

$$
\begin{bmatrix} t_n \\ t_s \\ t_t \end{bmatrix} = \begin{bmatrix} K_{nn} & K_{ns} & K_{nt} \\ K_{ns} & K_{ss} & K_{st} \\ K_{nt} & K_{st} & K_{tt} \end{bmatrix} \begin{bmatrix} \epsilon_n \\ \epsilon_s \\ \epsilon_t \end{bmatrix}
\tag{7.3}
$$

t is the nominal stress vector and K is the stiffness matrix. The force components divided by the original area at each integration point gives the nominal stresses. The nominal strains are given by

$$
\epsilon_n = \frac{\delta_n}{T_0}, \epsilon_s = \frac{\delta_s}{T_0}, \epsilon_t = \frac{\delta_t}{T_0}
\tag{7.4}
$$

Where T_0 is the original thickness of the cohesive element. An illustration of K is shown in figure 7.8.

The traction-separation behavior can be coupled or uncoupled. When uncoupled K_{nn}, K_{ss}, and K_{tt}, have to be defined and when coupled all nine components in the stiffness matrix have to be defined. If K_{ss} and K_{tt} in the uncoupled case is set to zero the cohesive behavior only acts in the contact normal direction and if K_{nn} is set to zero the normal separations will not be constrained.
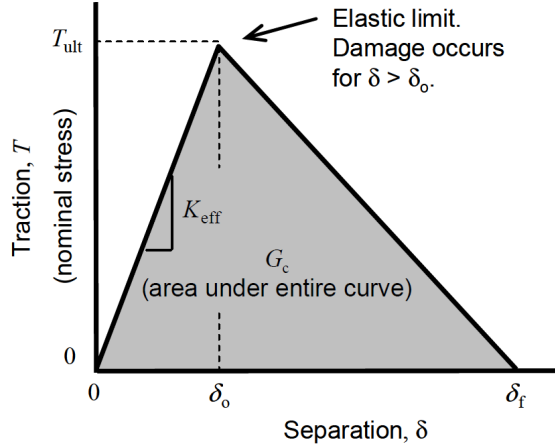
Figure 7.8: Traction-separation curve [20].
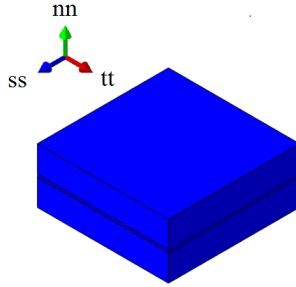
Figure 7.9: Directions in ABAQUS.

For cohesive elements there are six different ways to define the damage initiation law. In the simulations the quadratic sum of the ratios between nominal stress and maximum stress was used. When the sum reaches 1, damage is initiated. This damage initiation law is called Quads and was chosen since it is reasonable that the traction in the different directions interact during loading. Quads is given by

$$\left\{ \frac{\langle t_n \rangle}{t_n^o} \right\}^2 + \left\{ \frac{t_s}{t_s^o} \right\}^2 + \left\{ \frac{t_t}{t_t^o} \right\}^2 = 1 \tag{7.5}$$

The maximum stress in shear for the cohesive behavior was set to 2-3 times the normal maximum. If no damage evolution law is defined the damage process will not be modeled, but in the output it is showed whether or not the damage initiation criteria has been met. A value of 1 or higher indicates that the damage is initiated.

Damage evolution

Once the traction-separation behavior reaches the damage initiation criterion degradation of the cohesive response at a contact point is initiated and damage develops according to a damage evolution law, if defined. The damage evolution law describes the shape of the traction-separation curve after damage initiation. The shape of the damage evolution can be linear, exponential or user defined. A number of different damage mechanisms can act on the same material simultaneously. Cohesive elements do not undergo damage if the load case is pure compression. Damage initiation is either displacement driven or energy driven. Both options yield the same results when corresponding values are inserted, [19]. The simulations were made energy driven and the fracture energy, G_c, had to be given. Fracture energy was chosen since it was assumed to be obtained from the experimental tests.

When describing the shape of the curve a damage variable D is used. The variable has the value of 0 until damage is initiated and after that it evolves until it reaches the value of 1. It is calculated with

$$
t_n = \begin{cases} (1-D)\,\bar{t_n}, & \bar{t_n} \geq 0 \\ \bar{t_n}, & \end{cases}
\tag{7.6}
$$

$$
t_s = (1-D)\,\bar{t_s},
\tag{7.7}
$$

$$
t_t = (1-D)\,\bar{t_t},
\tag{7.8}
$$

When a combination of normal and shear separations is in question the effective separation can be used and is given by

$$
\delta_m = \sqrt{\langle \delta_n \rangle^2 + \delta_s^2 + \delta_t^2}
\tag{7.9}
$$

To specify the relative proportion between normal and shear separation, so called mode mix, energy or traction can be used. When energy is used, as in the simulations, the expressions becomes

$$m_1 = \frac{G_n}{G_T} \tag{7.10}$$

$$m_2 = \frac{G_s}{G_T} \tag{7.11}$$

$$m_3 = \frac{G_t}{G_T} \tag{7.12}$$

Where G_n, G_s and G_t are the work done by the traction in the normal and two shear directions. G_T is the sum of these three. m_1, m_2 and m_3 are used when specifying material properties related to damage evolution.

The evolution of D after damage initiation is called softening. A linear or exponential is possible.

Linear damage evolution is the easiest to describe and understand mathematically and was used in the simulations. It gives a realistic stress distribution in the peel front when the damage initiation is triggered early. The damage variable is calculated with

$$D = \frac{\delta^f{}_m(\delta^{max}{}_m - \delta^o{}_m)}{\delta^{max}{}_m(\delta^f{}_m - \delta^o{}_m)} \tag{7.13}$$

δ_m^{max} is the maximum value of the effective displacement during the loading history. $\delta_m^f = 2G^C/T_{eff}{}^0$ where $T_{eff}{}^0$ is the effective traction at damage initiation.

Mixed mode behavior

There are four different ways to model the mixed mode behavior; Mode independent, Tabular, Power law and Benzeggagh-Kenane (BK). The mode mix is the way the cohesive behavior evolve when it is subjected to forces in different directions. Power law was chosen in the simulations.

The power law criteria take into account that each direction has its own failure energy. How the different directions depends on each other can be manipulated with a power factor.

$$\left\{ \frac{G_n}{G^C} \right\}^n + \left\{ \frac{G_s}{G^C} \right\}^n + \left\{ \frac{G_t}{G^C} \right\}^n = 1 \tag{7.14}$$

58

An assumption was made that the release energy was equal in all directions. Power law with the power of 1 was chosen because little understanding of how the energies from failure in the normal and shear direction interacts was held. With power 1 the failure energy will always be the same independent of how the failure modes interact.

Degradation

There are two options for how the material will degrade compared to other damaging parameters than cohesive. These are maximum and multiplicative degradation. Maximum degradation chooses the highest degradation with no account to other damaging factors. Multiplicative degradation takes all damaging factors into account when damaging the material. Maximum degradation was chosen in the simulations.

7.5.3 Cohesive elements- Mesh

A cohesive element must be meshed in a specific way for the properties of the element to work as intended. The element can only fail in the thickness direction. A cohesive element, without the sub option pore pressure, have displacements only in its degrees of freedom.

Cohesive elements can be used in 3D, 2D and axisymmetric problems. When defining the element type in the input file the following procedure is used. COH3D8 is read as a cohesive element (COH) in 3D (3D) with 8 nodes (8). The letter P in the end will include pore pressure in the element, COH3D8P.
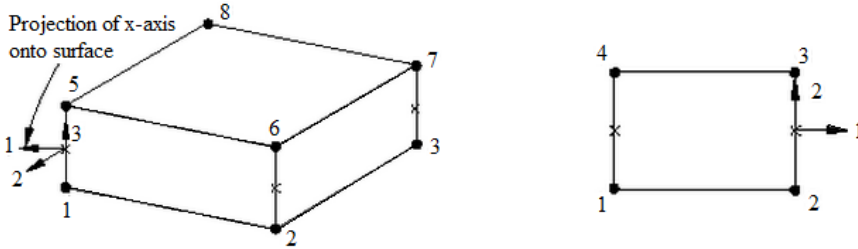
Figure 7.10: Element directions [19].

The layer of cohesive elements should not be more than one element thick. The tie interaction is the standard way to connect the cohesive elements with the adjacent parts, tie was used during the simulations. Other interactions can be used if a different behavior is wanted.

If the cohesive elements are small and has a low stiffness; the two parts on

59

each side of the cohesive element can move into each other. This is never a realistic solution and can be avoided by creating an interaction between the two parts.

A 3D traction element has stiffness in three directions, the normal direction and two shear directions. The stiffness is calculated from the material data E, G_1, G_2 and the thickness. The numerical thickness of the layer does not need to be the same as the thickness of the visual geometry in ABAQUS. The easiest way to get the wanted stiffness is to choose the default setting for thickness, which gives it the thickness 1. This means that you can treat E, G_1, G_2 as K_{nn}, K_{ss}, K_{tt}.

Chapter 8

Finite-Element study of adhesion

This chapter describes how the FE-models were developed for numerical studies of the peel tests performed. Since the plateau of the peel force is the only certain parameter that can be evaluated from the peel tests, this is what the simulations were aimed to correspond with. The deformations of the peel front were also compared with the purpose of verifying results. Unreliable results from simulations of Adhesion 1 led to that Adhesion 2 was focused on.

Simulations were first made for a 90° peel test for M2 and Adhesion 2, then a 180° peel test was made to investigate if the behavior of the adhesive produced the correct peel force for this angle as well. After this, geometry changes were made to simulate the other package materials, M1 and M3. How changes in the adhesion parameters affects the peel force were also tested. Mesh size dependency of the cohesive layer were also studied to investigate how it affects the results.

8.1 Finite-Element Model

The model was built in [mm] instead of [m] since it allows the desired precision of the geometry in the CAE. The reason to choose ABAQUS/Standard over ABAQUS/Explicit was because it produces a higher credibility in the solution. The material layers are very thin and the mesh needs to be dense to capture the proper bending, this would lead to very time consuming simulations for ABAQUS/Explicit.

It would be ideal to simulate the geometry of a full size experiment in 3D. Then the deformations in CD and the extension of the peel arm could be properly captured. The correct stress distribution with forces in CD would also be captured. The model was made in 2D and plane strain to get affordable simulation times. Neither plane strain nor plain stress is correct but plain strain has more in common with the test geometry. 2D works well when simulating Adhesion 2 since the deformation in CD is negligible. 2D was not as good for Adhesion 1 since the peel arm deforms in CD which results in a contraction force in CD.

The initial length of the layer that is to be peeled off is 1 mm in the model, the initial length of the peel arm is also 1 mm for Adhesion 2. For Adhesion 1 the peel arm is 0.5 mm because it does not need to be as long to capture the bending since it is less stiff and this decreases the simulation times. Experimental tests with short peel arm has been carried out to ensure that the length of the peel arm does not affect the plateau value of the force. The reason for not simulating a full scale experimental test specimen is that simulation times would become too long. The plateau force from the experimental tests are compared with the simulation results and these are not affected by the model length.
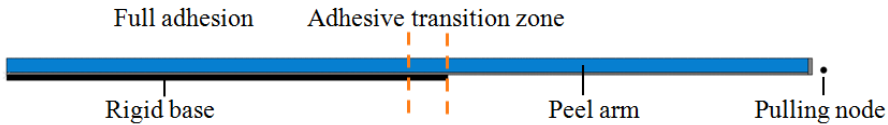
Figure 8.1: Undeformed model for simulating Adhesion 2.

If the element deformations are small, as when Adhesion 2 was simulated, then quadratic elements are preferred. When Adhesion 1 is simulated the deformations in the lower elements are so large that triangle elements are preferred. The peel arm was meshed dense enough to capture the bending correctly. The cohesive layer was meshed dense enough to capture the stress distribution at the peel front and to avoid fluctuating peel force.

To smoothen the transition between the material of the initial peel arm, that was not plasticized, and the material that plasticize during crack propagation 10 transition zones have been made in the cohesive layer. The adhesion increases linearly over the transition zones.

The simulations were performed displacement controlled to make them stable, a force controlled simulation would fail once the plateau force is reached. The model includes the nonlinear effects of large deformations and displacements. When needed, global stabilization was used. Damping was avoided as far as
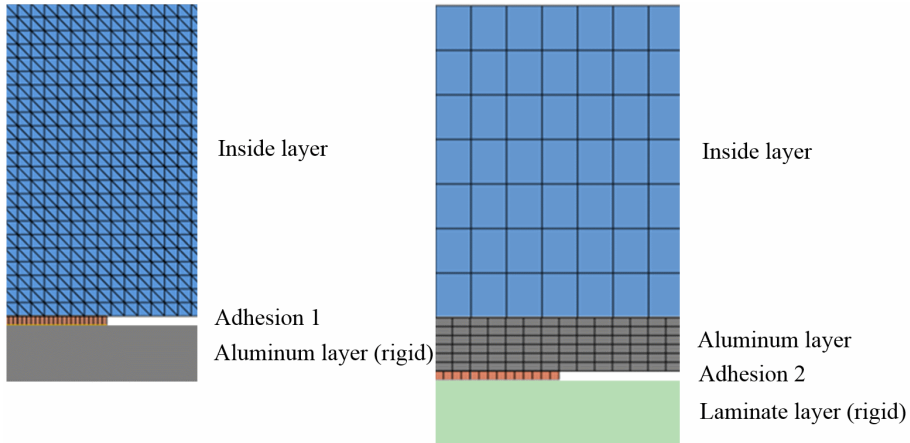
Figure 8.2: Undeformed mesh at the peel front.

possible since it could affect the result if implemented poorly.

Simulations were made for M2 in 0° for Adhesion 1 and 90° for Adhesion 2 until the adhesion behaviors produced the correct plateau forces. Then the angles 0°, 90° and 180° were tested for the package materials M1, M2 and M3 for both Adhesion 1 and Adhesion 2. This was done with the previously determined adhesion properties.

8.2 Results

Instability was at some point reached in all simulations. The simulation results presented in graphs have all been aborted due to stability errors. This results in that some of the graphs does not show a clear plateau force or are shorter than others.

8.2.1 Adhesion 1

The values shown in table 8.1 are obtained from the simulation of 0° and M2 that corresponds well with the plateau force of the experimental test even though the deformations of the peel arm does not visually correspond. The peel arm does not extend enough in the simulation which may be because the simulation is done in 2D which does not allow deformations in CD. Figure 8.6 shows that even though the extension of the peel arm is wrong the difference in force between simulations and experimental results is not large. M1 and M2 has the same geometry of the peel arm so they will give the same results, therefore M1 was not simulated.

Adhesion 1			
Setting	nn	ss	tt
σ_{max} [MPa]	10	20	20
K [GPa]	80 000	300 000	300 000
G_c [J/m^2]	25	25	25
Damage Initiation	Quads		
Damage Evolution	Linear, Power Law 1		

Table 8.1: Settings for cohesive behavior, Adhesion 1.
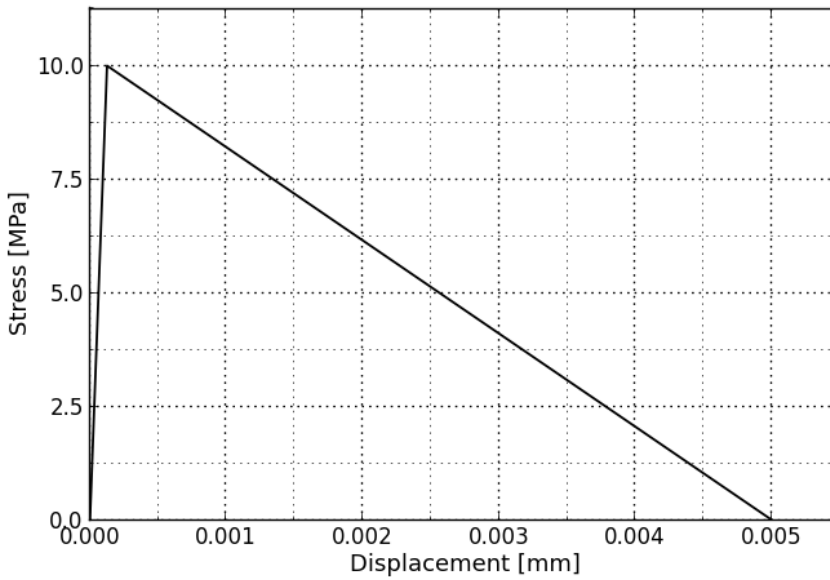
Figure 8.3: Adhesion 1. Traction-separation behavior, normal direction.

Figure 8.4: Deformed model, Adhesion 1.

Attempts were made to make simulations for 90°, with the same material parameters as for 0°. Attempts were also made for 0° using the other material parameters for the Inside layer, the set with lower E-module, see chapter 7. It was not possible to get any clear results.
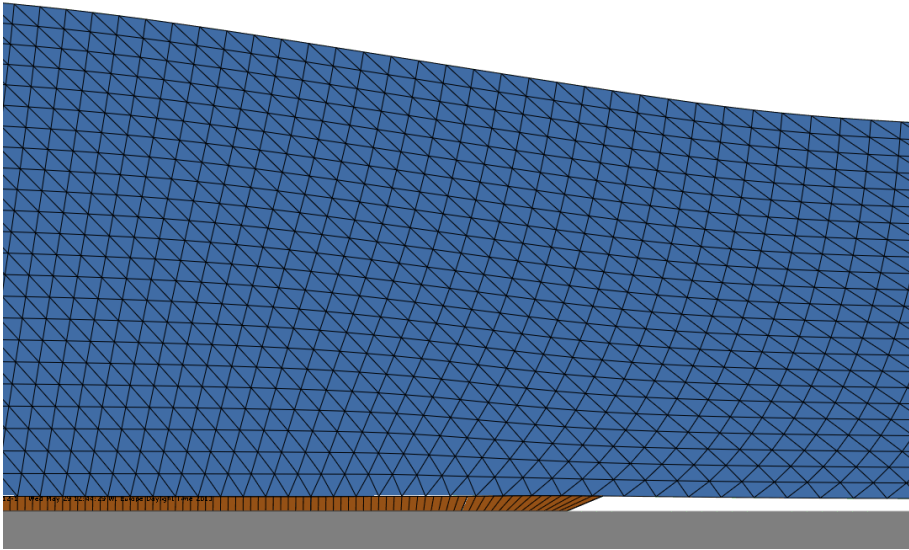
Figure 8.5: Peel front during plateau force 0°, Adhesion 1.
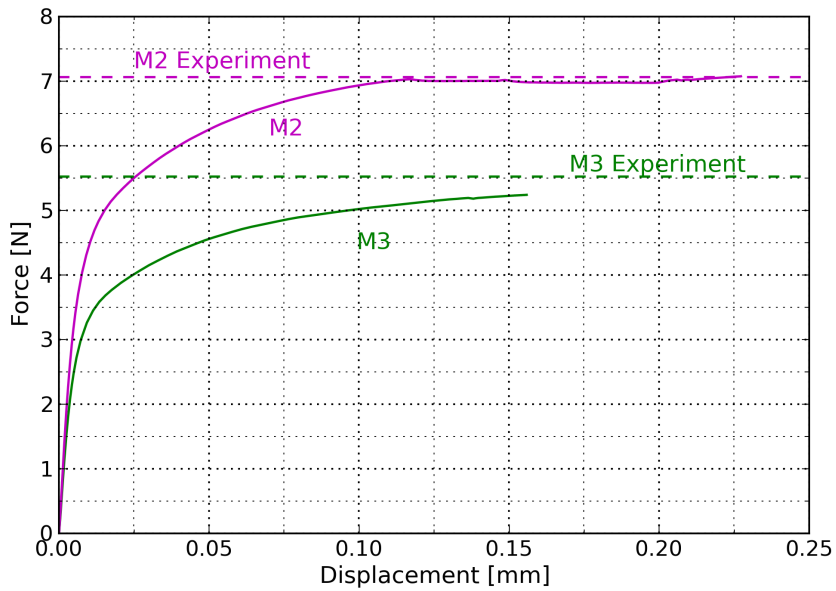
Figure 8.6: Simulations in ABAQUS for Adhesion 1, 0°.

8.2.2 Adhesion 2

The values in table 8.2 are calibrated to produce the same peel force as the experimental test in 90° for M2. Corresponding traction-separation curve, in normal direction, is illustrated in figure 8.7.

Adhesion 2			
Setting	nn	ss	tt
σ_{max} [MPa]	15	30	30
K [GPa/m]	40 000	80 000	80 000
G_c [J/m^2]	36	36	36
Damage Initiation	Quads		
Damage Evolution	Linear, Power Law 1		

Table 8.2: Settings for cohesive behavior, Adhesion 2.
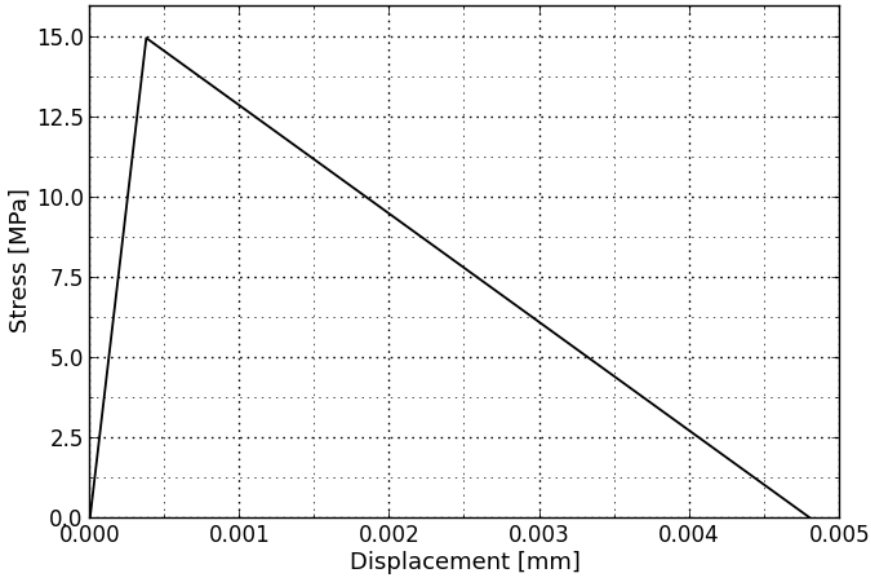
Figure 8.7: Adhesion 2. Traction-separation behavior, normal direction.

The same adhesion parameters were used for M1 and M3 as well and the results are shown in figure 8.9 and figure 8.10. The numerical simulations for M2 were done using global stabilization. The dissipated energy fraction was 0.0002 with an adaptive stabilization that had a maximum ratio of stabilization to strain energy of 0.05. The use of damping resulted in peaks in the graphs. Since it is the plateau value for the peel force that is of interest,

no in-depth analysis of the damping effects was made. M1 has thicker Aluminum layer and the results shows that the peel force in both angles are higher for this package material. The reason for the curves not beginning at 0 N in figure 8.10 is that the pulling node is pressed towards the peel front until the peel arm buckles. Figure 8.8 shows the deformations of the peel arm at the peel front. A visual comparison of simulation and experimental test shows that the deformations are similar, see 8.8. This confirms that the stiffness of the material was correct to some extent. The small bend in the peel arm, for the simulations, seen clearly in 90° and at the very top of the 180° is where the full adhesion started.

The peel forces shown in table 8.3 are all simulated with the calibrated adhesion parameters from M2, 90°. The reason why the simulation of M2, 90°, does not show the same value as the experimental test is because an inaccurate reading from the graph when the adhesion parameters was determined. The numerical simulations for M2 were done usinf global stabilization. The dissipated energy fraction was 0.0002 with an adaptive stabilization that had a maximum ratio of stabilization to strain energy of 0.05.

Peel force, adhesion 2			
	Experimental test	Numerical test	Difference
M1, 90°	1.38	1.52	+14%
M2, 90°	1.38	1.37	-1%
M3, 90°	1.45	1.38	-5%
M1, 180°	1.18	1.38	+17%
M2, 180°	1.18	1.19	+1%
M3, 180°	1.24	1.22	+2%

Table 8.3: Comparison of experimental tests versus numerical simulations.

90°

180°

Numerical results   Experimental results
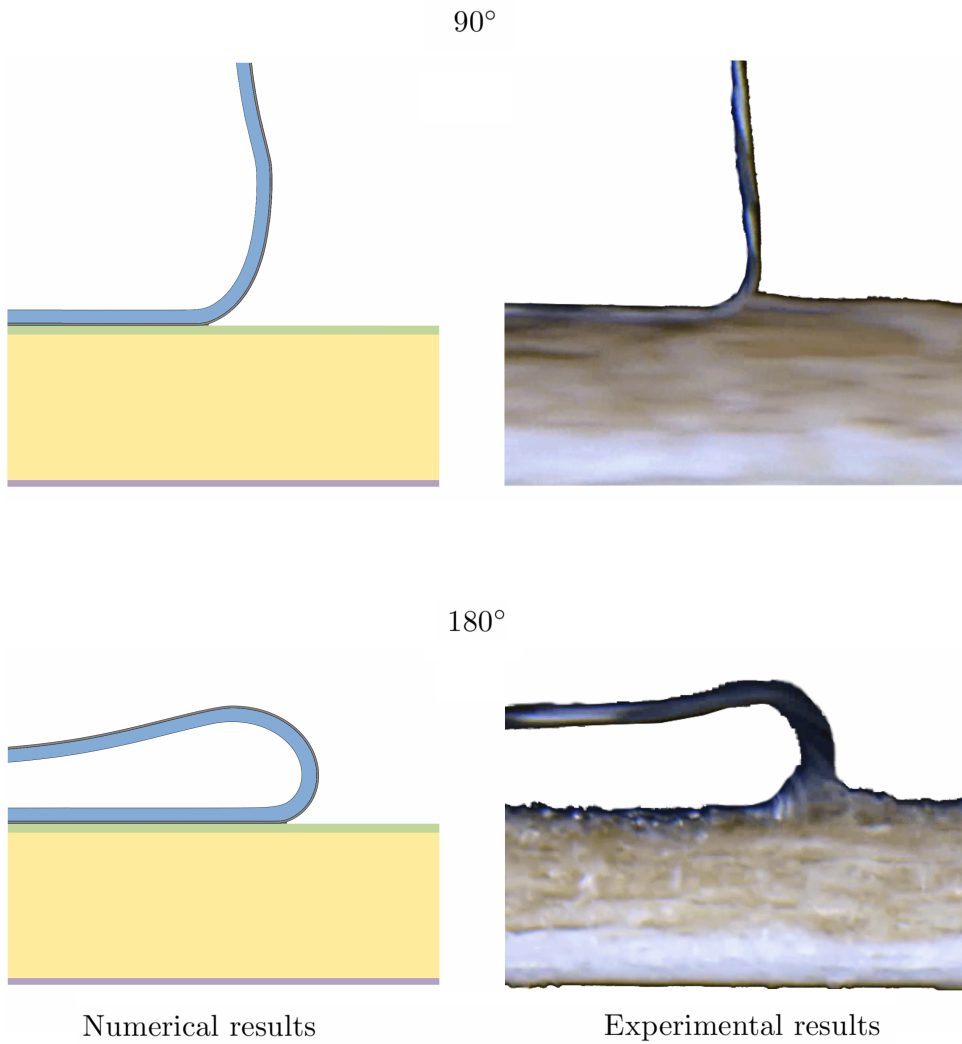
Figure 8.8: Visual comparison of deformations for M2, Adhesion 2; Inside-
and Aluminum layer.
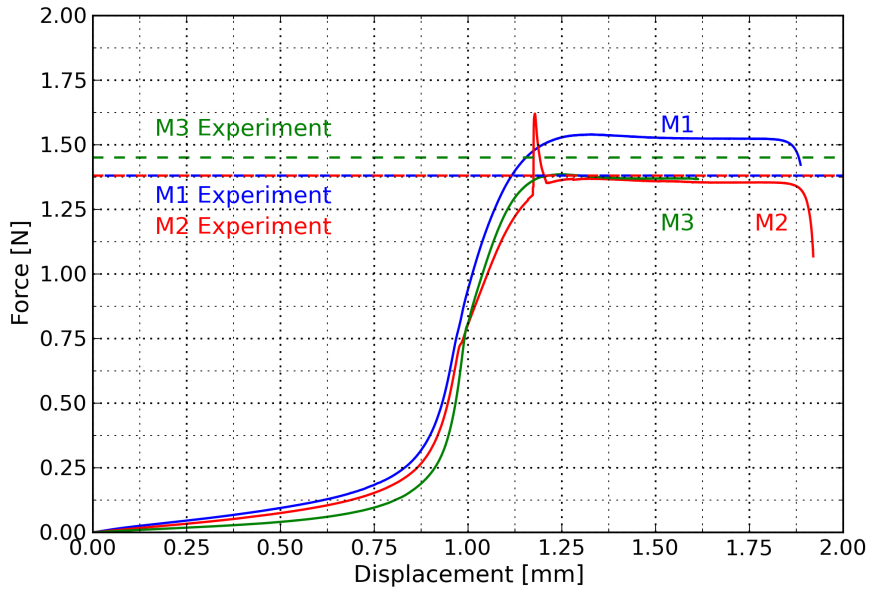
Figure 8.9: Simulations in ABAQUS for Adhesion 2, 90°.
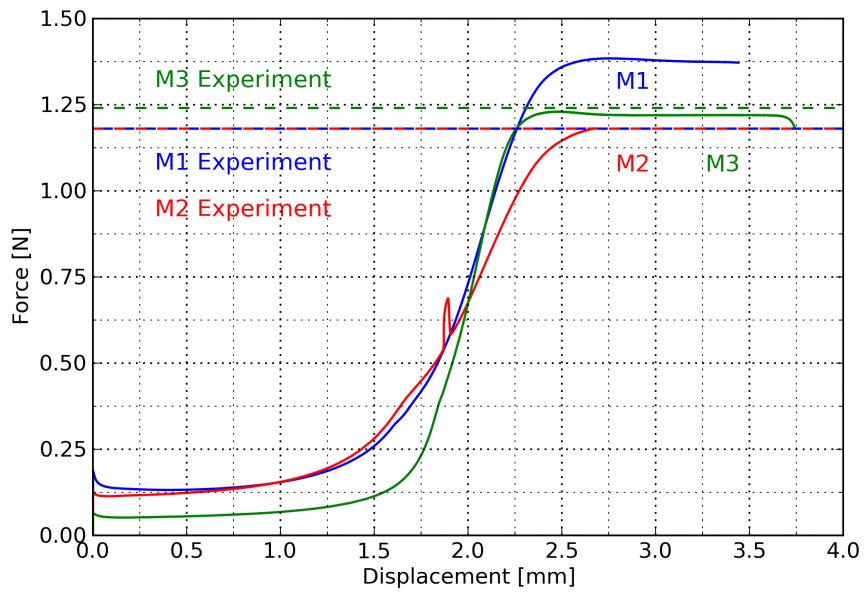
Figure 8.10: Simulations in ABAQUS for Adhesion 2, 180°.

The result of changes in the adhesive behavior is shown in figure 8.11 and a visual image of the different adhesive properties is shown in figure 8.12.
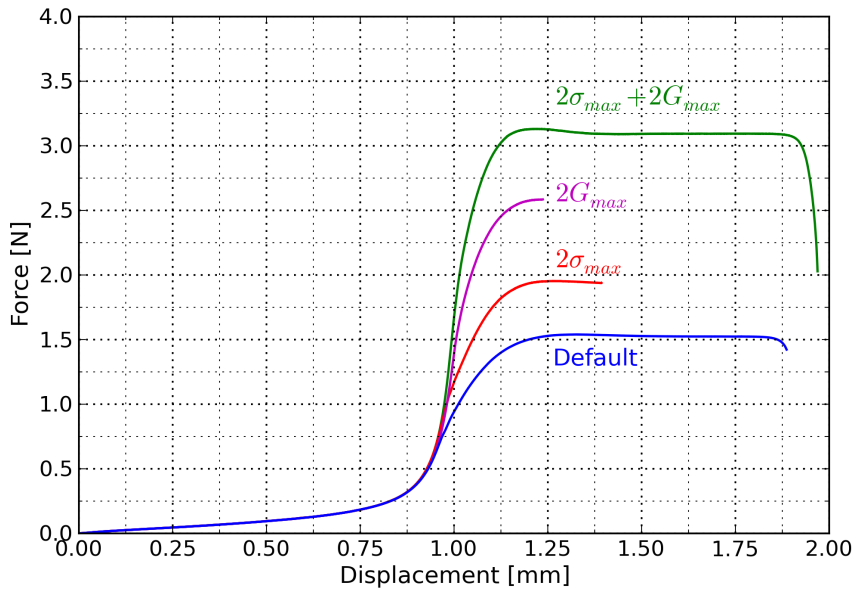
Figure 8.11: Results for different adhesion properties for M1, 90°.
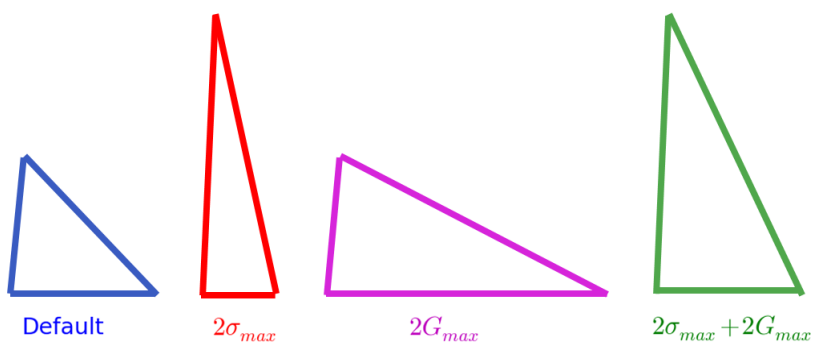
Figure 8.12: Shape of the different traction/seperation settings in figure 8.11.

The result from investigating mesh size versus release distance is presented in figure 8.13. A mesh ratio of 0.2 was used in the standard model which means that the width of one cohesive element is 0.2 times the release distance of the adhesive properties. The release distance is defined as the distance at which the adhesion stress in the normal direction becomes zero. It can clearly be seen that a high mesh ratio results in a jagged curve. To avoid unwanted peeks in separation force in future applications, the width of the cohesive elements should not be over 0.5 times the release distance for the cohesive behavior in the normal direction. There is no exact limit of how small the cohesive element should be since it differs with different peel arms.
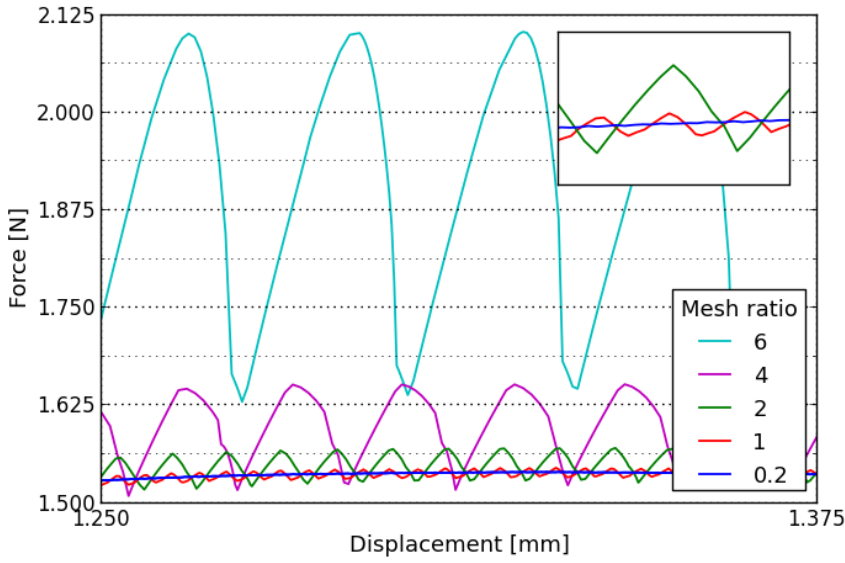
Figure 8.13: Different ratios of release distance divided by mesh size for 90°, M1.
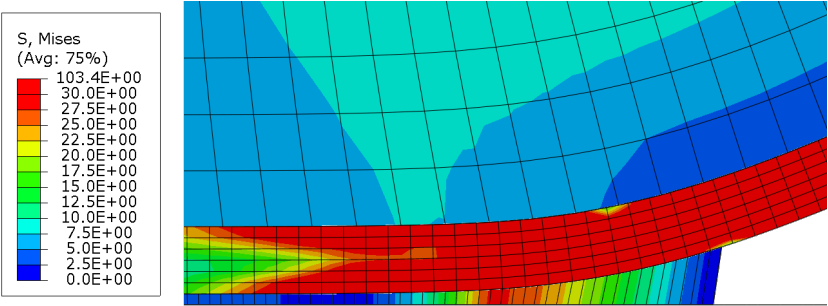
Figure 8.14: Stress distribution in the cohesive layer for Adhesion 2.

8.3   Discussion

The layers in the peel arm are subjected to a serie of loads that deforms them plastically. Isotropic hardening models were used for all layers in the model, further studies should be done to reach a correct hardening model. For simulations in 90° and 180° the material on the upper side of the peel front is first subjected to pressure and later to tension. The material in the lower part of the peel front is first subjected to a large tensile force which then decreases, see figure 8.15. This can result in unrealistic stress distribution in the peel arm. This hardening of the upper side can hinder necking in the simulations that occurs in the experimental tests.
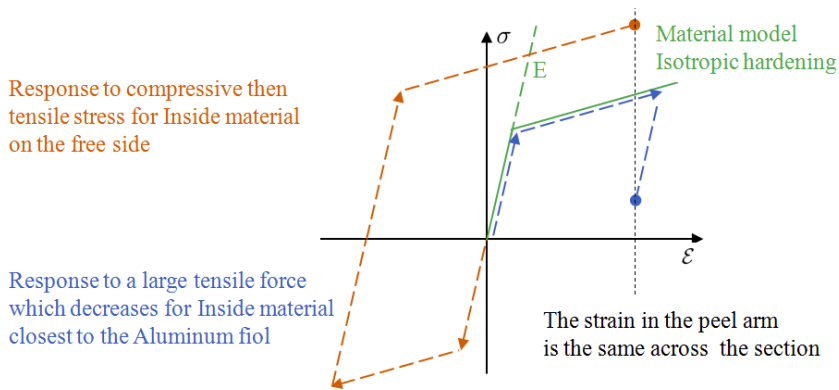
Figure 8.15: Isotropic responce.

Another aspect that isotropic hardening affects is the energy used to make plastic deformations. When a major part of the purpose of the simulation is to determine the energy used to break the adhesion a material model which plasticize wrongly can affect the result. The most time efficient way of improving the entire model would probably be to discuss combined hardening with material experts and implement the conclusions.

An uncertainty with the Inside layer is that Young's modulus is changing during the increasing strain of the material, this is not included in the model. Young's modulus affects the amount of strain that is plastic, which affects the energy consumed when the material plasticizes.

8.3.1   Adhesion 1

Since the peel arm does not extend as much as it should in the simulations; the amount of inserted energy is to low. The peel front seen in figure 8.5 looks realistic for a material that only extends a short bit. The release distance of the adhesion looks reasonable but it is hard to validate.

The material parameters used for the Inside layer is the set with the high E-modulus. This should work well for 0° and isotropic hardening since there is almost exclusively tensile forces in the model and no cyclic loading. 90° and 180° would work badly with isotropic hardening since there are very large deformations in the peel arm, the reason is described in figure 8.15. A stiff E-modulus will increase the fault from the isotropic hardening in cyclic loading. No reliable results was found for simulation in 90°.

8.3.2 Adhesion 2

The peel force for M2, 180°, is very close to the result from the experimental tests, this indicates that the peel forces can be predicted in different angles once one of the angles adhesive properties have been calibrated.

For both 90° and 180° M1 results in a higher peel force than M2 and M3. The assumption that the adhesion is the same in all angles is reasonable since the adhesive behavior itself is not affected by the peel angle.

It was more difficult for M2 simulations to reach the plateau values, this could be due to that M2 has the largest ratio of Inside layer compared to the Aluminum layer.

The result that the curves get more peaks as the mesh ratio increase is consistent with what can be expected. The ratio that gives a smooth curve corresponds to the findings by Ted Diehl, in [20]. It is not the ratio itself that is the critical factor but the number of active adhesive connectors. This makes the geometry and stiffness of the peel arm a factor when trying to find the optimal mesh size. The same principle that enough connectors should be active is assumed to apply for shear loads too, for example 0°.

To mesh the cohesive elements small enough is not a problem for a model of the size used here. For bigger models a mesh as small as this results in long simulation times. One untested way to work around this is to lower the maximum stress and include the plasticization energy into the separation energy, this will increase the release distance while capturing the plasticization energy in the peel front that otherwise would have been lost in a bigger mesh. A full size 3D model would probably use larger shell elements for the structure so the material would not be able to bend and plasticize which should dissipate energy. How these two factors affects the result is uncertain and has not been studied in this report.

It is hard to evaluate the reliability of the input parameters for the adhesive behavior. Other combinations could give the same plateau force. That the

used combination gives the correct force in two angles is a good indicator that the model is correct to some degree for the simplifications that were made. To be convinced about exactly how the damage evolution should be modelled more studies have to be made to determine the adhesive behavior.

When the maximum stress of the adhesion is doubled, but the separation energy is still as for the default setting, the peel force increases about 30%. This is more than anticipated, the extra amount of inserted energy is dissipated into plastic strains since the elements closest to the peelfront is now subjected to a near twice as large stress.

When the separation energy is doubled and the maximum stress is as default the peel force increases about 70% which seems reasonable. When both the separation energy and maximum stress limit is doubled the peel force increases about 100%. This indicates that the result of different parameter changes are additive.

The length of the curve for double stress and energy is a little longer than the curve for the default settings in figure 8.11. This is because the force is higher which gives a higher amount of strain in the peel arm.

To get a more correct shape of the peel arm the material in the initial peel arm has to be given the correct material parameters. This part of the Inside layer and Aluminum layer has already plasticized during specimen preparation so comparing the incline before the plateau value between experimental tests and numerical test is unnecessary.

The material models can be a contributing factor to the instability with strange stress distributions and a non changing Young's modulus that stores too much elastic energy to be released.

To increase the release distance of the cohesive material is the easiest way to make it more stable but it is a bad approach to increase it beyond what is realistic. It is very hard to obtain the correct release distance since only pictures and movies are available to evaluate.

The peel force is very similar between M1 and M2 in the experimental tests but the simulations in ABAQUS gives that the thickness of the aluminum affects the results. This could be because the properties of the Aluminum layer are dependent on the thickness which is not included in the model. It is hard to evaluate the results from M3 since Adhesion 2 is prelaminated.

Figure 8.8 shows that the Paperboard layer delaminates, this is not included in the FE-model.

Chapter 9

Conclusions

The problem of determining the mechanical adhesion parameters is more complex than it might look at first sight. This study shows that a large number of properties have to be known before simulating the mechanical properties of the adhesion can be done correctly. Two factors that have an impact on peel tests but were very simplified in this study are the properties of the layer from which the peel arm is peeled off and the viscous properties of the adhesion strength.

Comparing adhesion strength from peel tests is challenging when different peel arms are used. The stiffness of the peel arm affects the stress distribution and the material properties of the peel arm affect the amount of dissipated energy. If comparable thicknesses and raw materials are used in the peel arm, the difference in results is probably originating from different adhesion strengths. The results from this study have to be verified further before applied.

It is possible to simulate adhesion strength in ABAQUS/Standard using cohesive elements. As previously seen in figure 8.9 and figure 8.10, one setting for the adhesion strength produces good results for two different loading conditions.

Energy is released when the adhesion strength is exceeded. This phenomenon is per definition an unstable and numerically challenging problem. Nevertheless was it possible to simulate the experimental peel test numerically at a very small scale in Abaqus/Standard, v.6.12. A dense mesh is needed to properly simulate the adhesion and to capture the proper deformations of the peel front. This would lead to extremely long simulation times if a full scale simulation was done in 3D.

When simulating Adhesion 1 in 0° the same adhesion properties were used for M2 as for M3. M3, which has a thinner peel arm, resulted in a lower peel force. If the result from the simulations came from an experimental test it would have been interpreted as the adhesion for M2 was the highest. This would be an incorrect statement since the adhesion in fact is exactly the same. This shows that it is not only the adhesion that is measured in the experimental tests. What is measured in peel tests is a combination of adhesion, geometry and material properties.

Chapter 10

Further work

If the adhesion is to be fully understood it would be preferred to start with the basics and get them right and work from there.

New test methods for testing the adhesion between thin layers on a small specimen need to be developed. These test methods should be able to test one fracture mode at the time and should also be able to test a combination of normal and shear stresses. A good estimation of the adhesion strength could be done with these methods.

Extensive testing should be made on the material of the Inside layer and Aluminum layer so the material models behave properly in cyclic loading. The Paperboard layer delaminates in z-direction during peel tests on package material. This dissipates energy and affects the angle of which the peel arm leaves the base, therefore a good material model is needed for this layer as well.

Once these parts are solved they should be put together in a complex problem, for example a peel test. When the result is good enough, then smaller problems could be solved and predicted in 2D simulations.

If adhesion is to be used in larger 3D simulations some sort of simplified model must be used due to extremely long simulation times if the correct behaviour is to be captured. It might be possible to incorporate the dissipated energy due to plasticization in the peel front into the separation energy. This can allow an increase of the mesh size since the proper deformation in the peel front no longer needs to be captured. An adjustment to make the release distance of the adhesion longer would also be needed due to larger elements. This will not be the "true" adhesion but might work for some applications.

If Tetra Pak had the possibility to compare peel test results from a large number of tests, with approximately the same peel arms, it would be interesting to compare the peel forces. If the peel forces are approximately the same for most tests the definite conclusion can be made that the geometry affects more than the differences in adhesion strength.

Bibliography

[1] N. Ottosen, H. Petersson *Introduction to the Finite Element Method* Prentice Hall 1992.

[2] S. Krenk *Non-linear Modeling and Analysis of Solids and Structures* Cambridge University Press 2009.

[3] L. F. M. da Silva, A. Öchsner, R. D. Adams *Handbook of Adhesive Technology, Chapter 1: Introduction to Adhesive Bonding Technology* Springer-Verlag Berlin Heidelberg 2011.

[4] D. E. Packham *Handbook of Adhesive Technology, Chapter 2: Theories of Fundamental Adhesion* Springer-Verlag Berlin Heidelberg 2011.

[5] M. Brogly *Handbook of Adhesive Technology, Chapter 3: Forces Involved in Adhesion* Springer-Verlag Berlin Heidelberg 2011.

[6] A.J. Kinloch *Adhesion and Adhesives: Science and Technology*, Chapman and Hall 1987.

[7] J. C. Berg *Adhesion Science and Engineering: Volume 1: The Mechanics of Adhesion, Chapter 1: Semi-empirical strategies for predicting adhesion* 2002.

[8] V.S. Mangipudi, A. Fasafi *Adhesion Science and Engineering: Volume 1: The Mechanics of Adhesion, Chapter 2: Direct estimation of the adhesion of solid polymers* Elsevier Science 2002.

[9] D.S. Rimai, D.J. Quesnel *Adhesion Science and Engineering: Volume 1: The Mechanics of Adhesion, Chapter 3: Particle adhesion* Elsevier Science 2002.

[10] A.J. Kinloch, J.G. Williams *Adhesion Science and Engineering: Volume 2: Surfaces, Chemistry and Applications, Chapter 8: The mechanics of peel tests* Elsevier Science 2002.

[11] J. Comyn *Adhesion Science* Royal Society of Chemistry 1997.

[12] C.C. Lau *A fracture mechanics approach to the adhesion of packaging laminates- A final report for Tetra Pak* Imperial College, 1993.

[13] P.J.G. Schreurs *Fracture Mechanics: Lecture notes - course 4A780* 2012.

[14] A. T. Travesa *Simulation of delamination in composites under quasistatic and fatigue loading using cohesive zone models* Universitat de Girona, 2006.

[15] *Fracture Mechanics* [http://www.scribd.com/doc/137452050/pm10-tisk], 2013-06-07.

[16] D. Dodrill *Advances in peelable sealant technology* [http://rollprint.com/PDF/PeelableSealants.pdf] 2013-06-07.

[17] L.F. Kawashita, D.R. Moore *ICPeel (2006)* Kinloch, Williams, Imperial College London 2006.

[18] J. Jönsson, M. Sandgren *Fracture mechanics in ductile plastics* Division of Solid Mechanics, Lund University, 2013.

[19] Dassault Systems *ABAQUS Analysis User's Manual 6.12* 2013.

[20] T.Diehl *Using ABAQUS Cohesive Elements to Model Peeling of an Epoxy-bonded Aluminum Strip: A Benchmark Study for Inelastic Peel Arms* DuPont, 2006.

[21] N.S. Ottosen, M. Ristinmaa *The Mechanics of Constitutive Modelling*, Volume I-II, Division of Solid Mechanics, Lund University, 2003. .

[22] F.Nilsson *Fracture Mechanics: From Theory to Applications*, KTH Hllfasthetslra, 2001.

Appendix A

Experimental test results

A.1   Adhesion 1
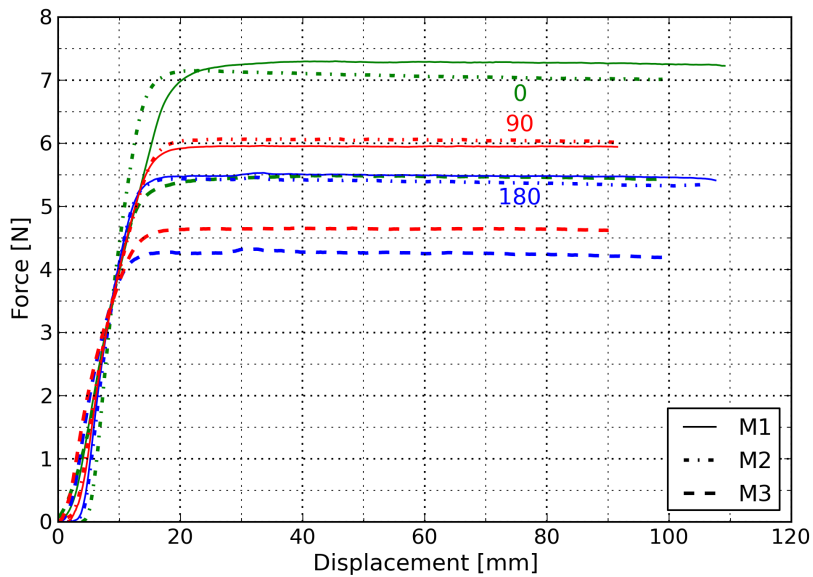
Figure A.1: Mean curves for Adhesion 1.
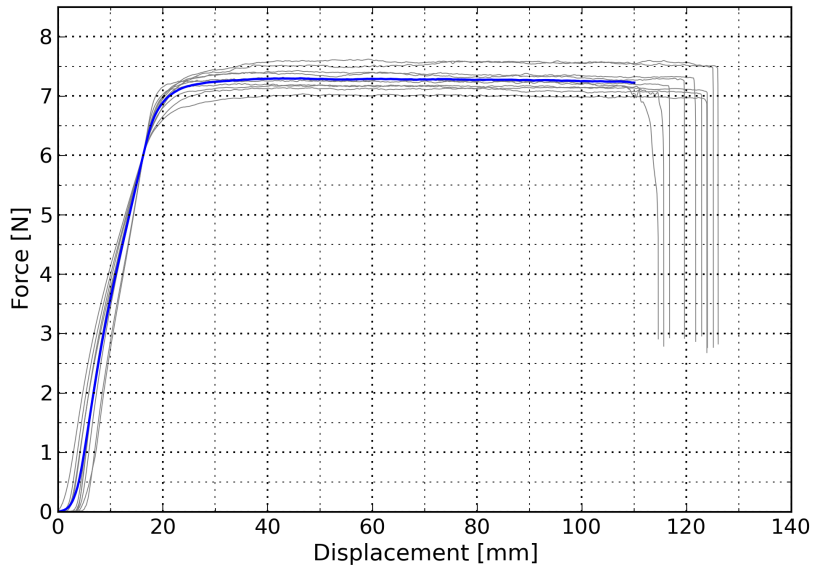
Figure A.2: Adhesion 1, 0°, M1.
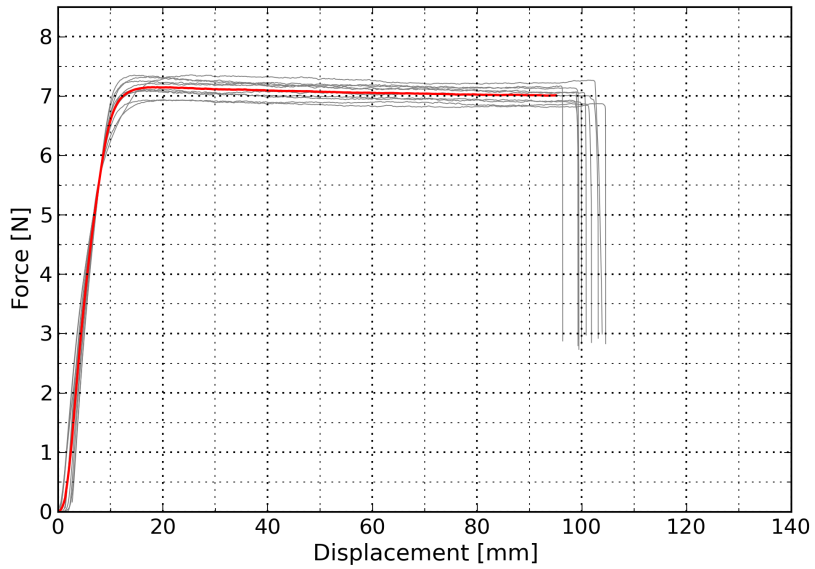
Figure A.3: Adhesion 1, 0°, M2.
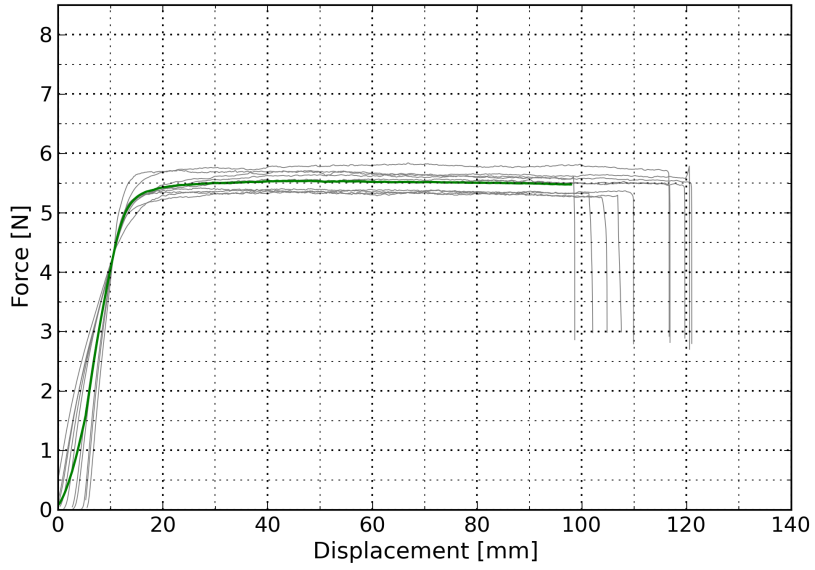
Figure A.4: Adhesion 1, 0°, M3.
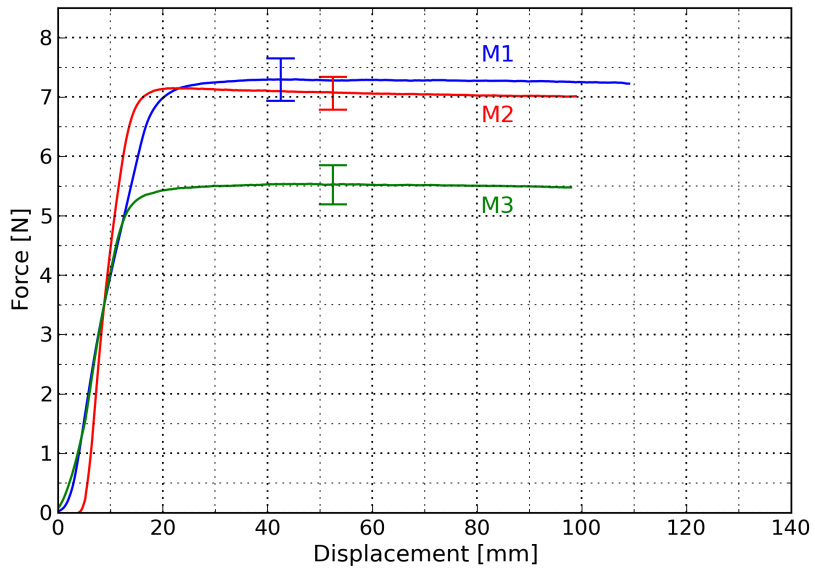
Figure A.5: Adhesion 1, 0°, mean curves.

## A.1.2 90° test
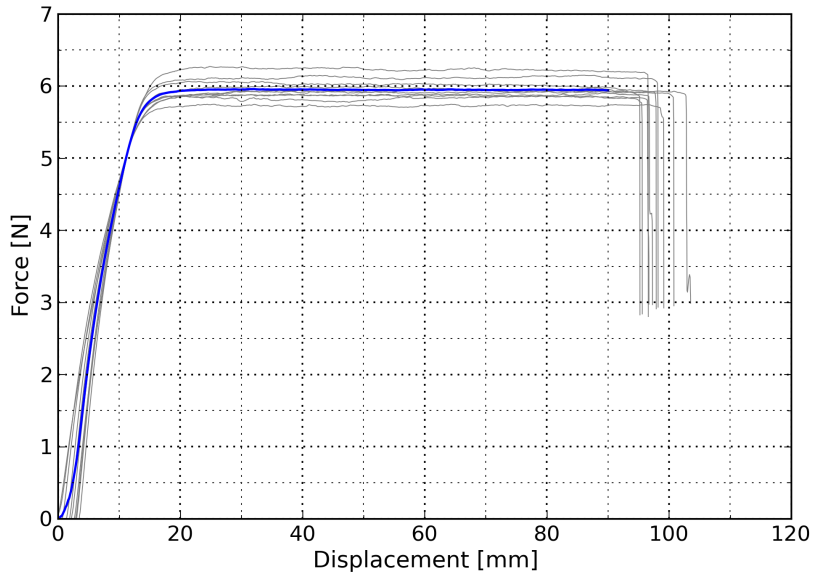
Figure A.6: Adhesion 1, 90°, M1.
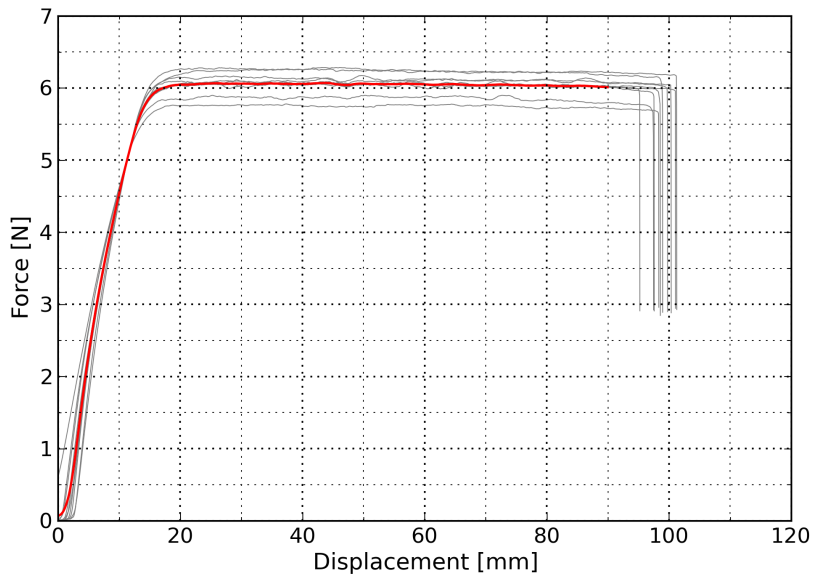
Figure A.7: Adhesion 1, 90°, M2.
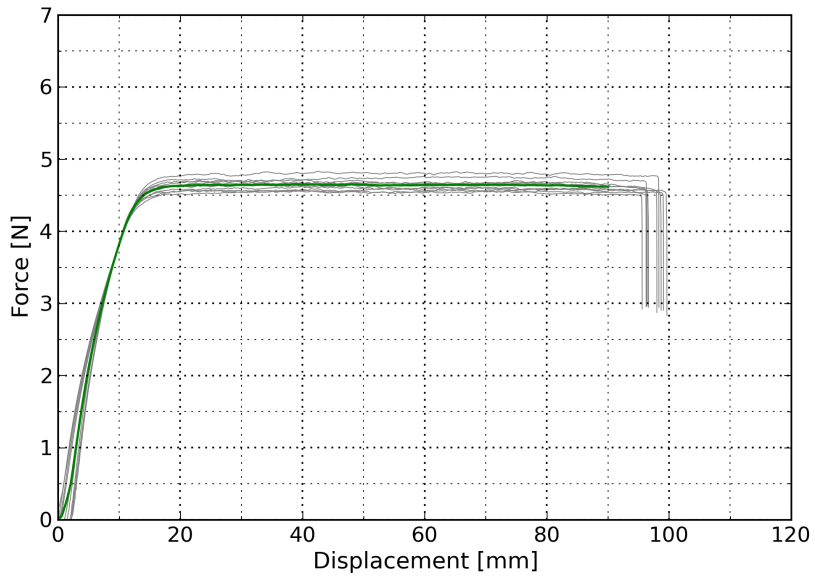
Figure A.8: Adhesion 1, 90°, M3.
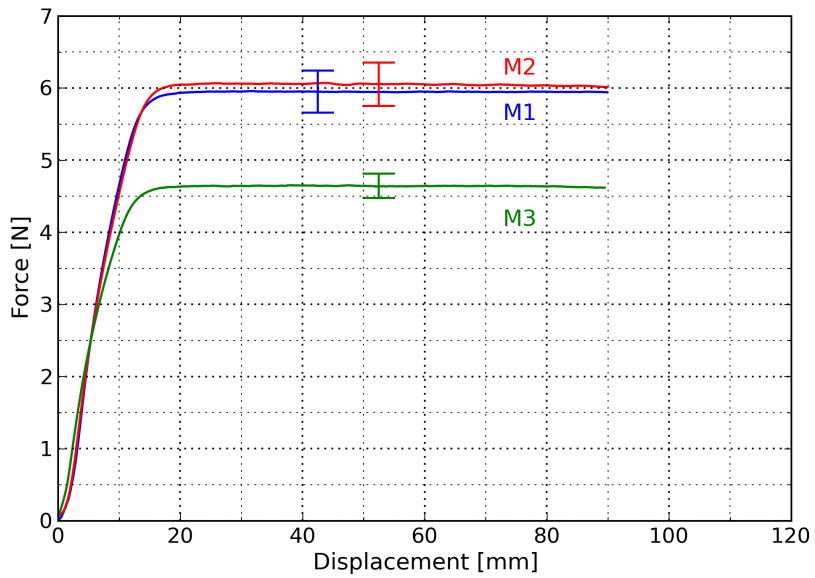
Figure A.9: Adhesion 1, 90°, mean curves.

A.1.3 180° test
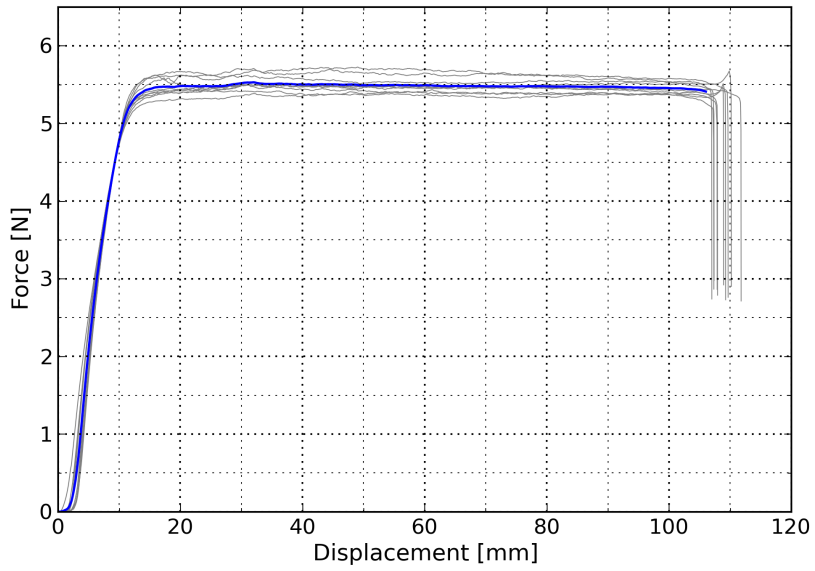
Figure A.10: Adhesion 1, 180°, M1.
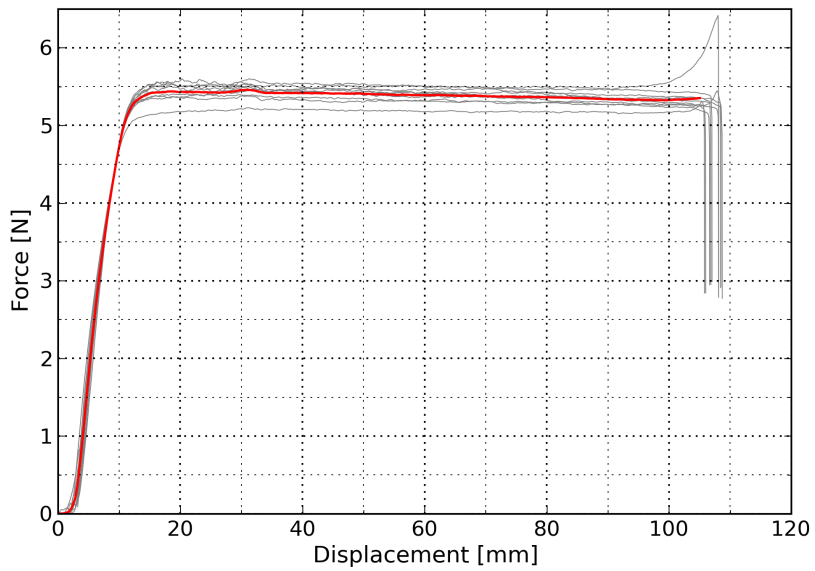
Figure A.11: Adhesion 1, 180°, M2.
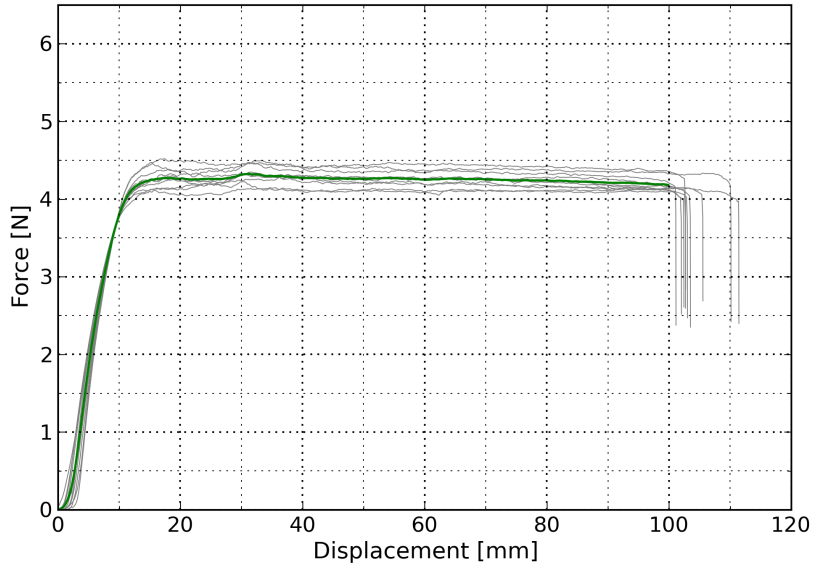
Figure A.12: Adhesion 1, 180°, M3.
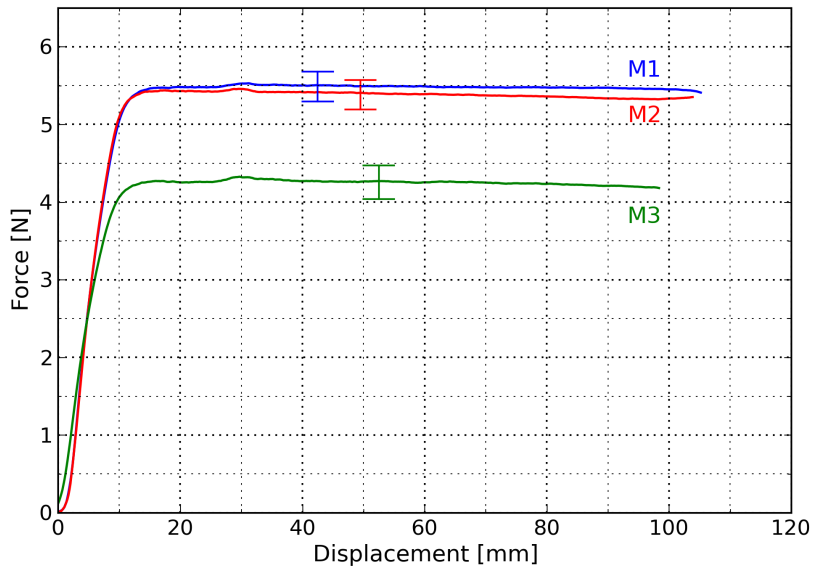
Figure A.13: Adhesion 1, 180°, mean curves.

A.2   Adhesion 2
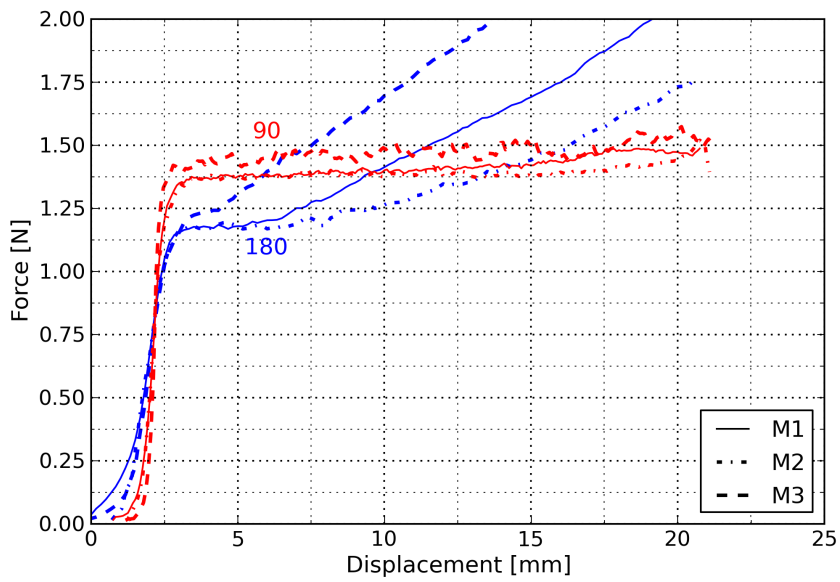
Figure A.14: Mean curves for Adhesion 2.
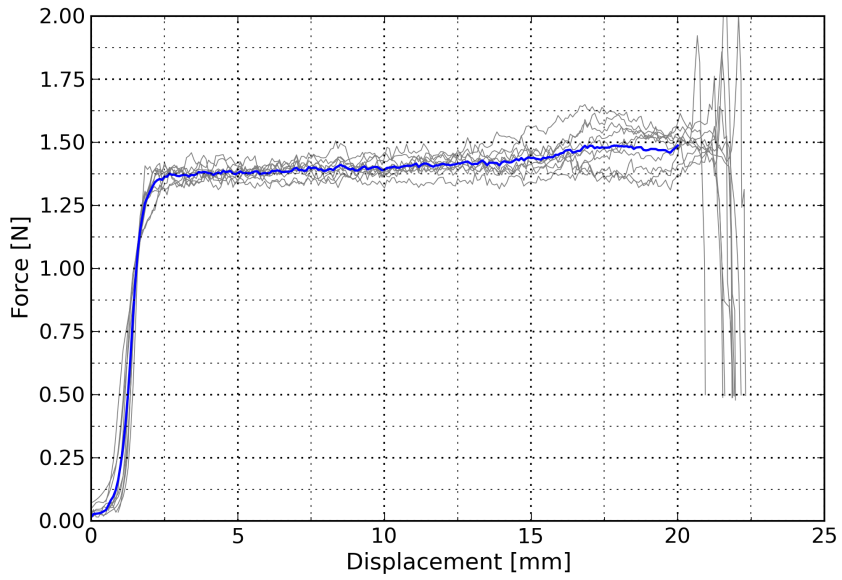
Figure A.15: Adhesion 2, 90°, M1.
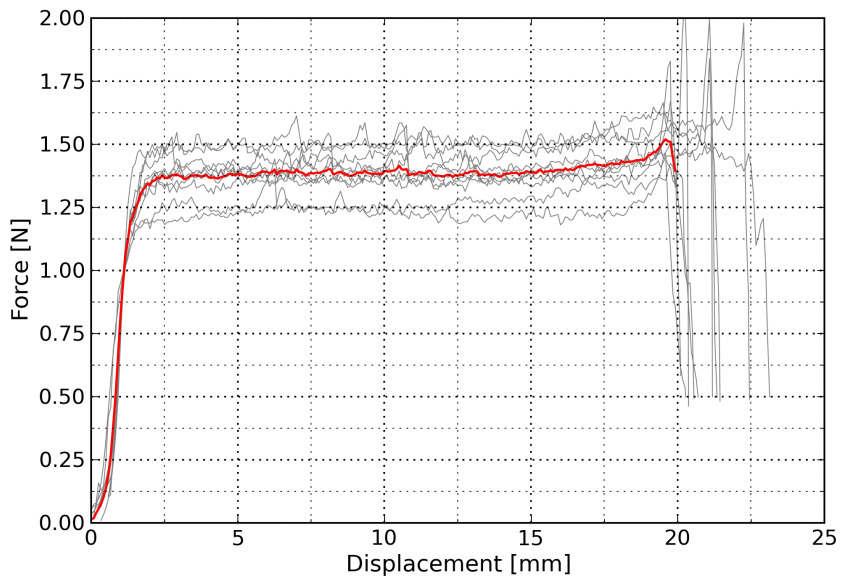
Figure A.16: Adhesion 2, 90°, M2.
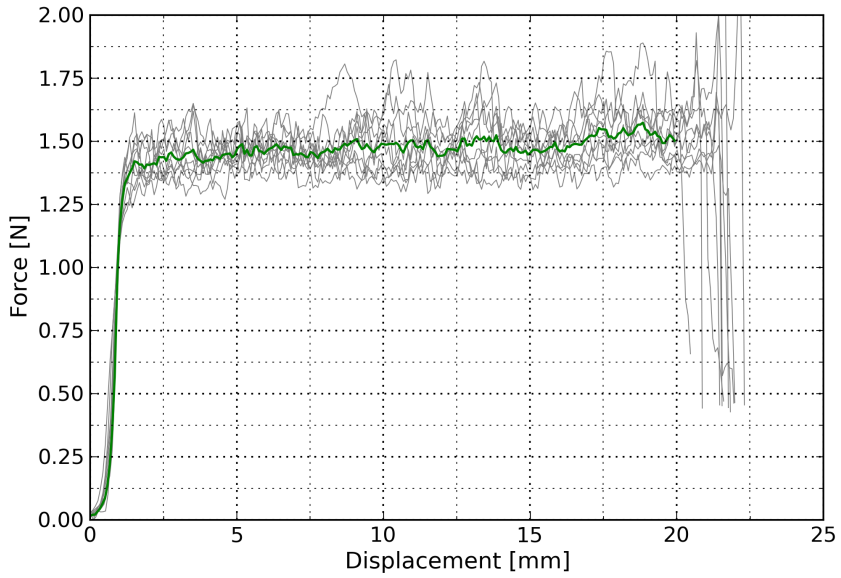
Figure A.17: Adhesion 2, 90°, M3.
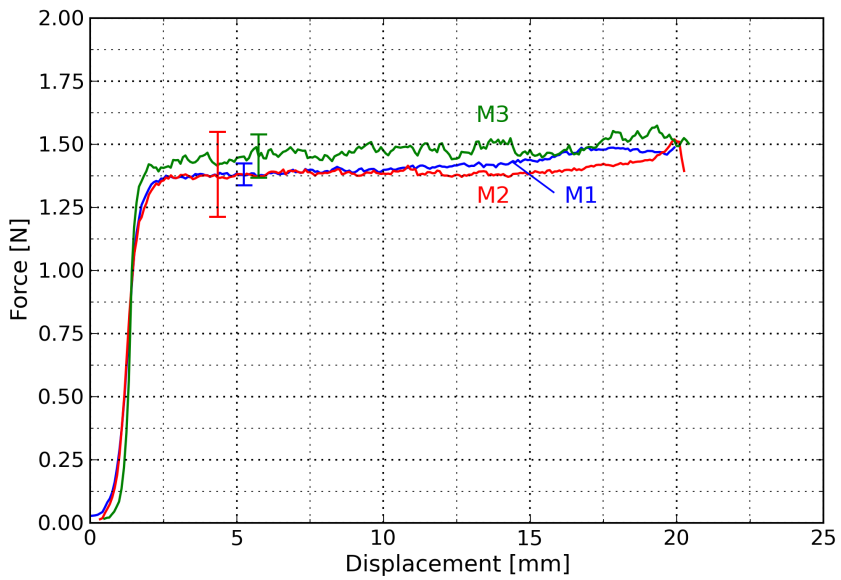
Figure A.18: Adhesion 2, 90°, mean curves.

A.2.2   180° test
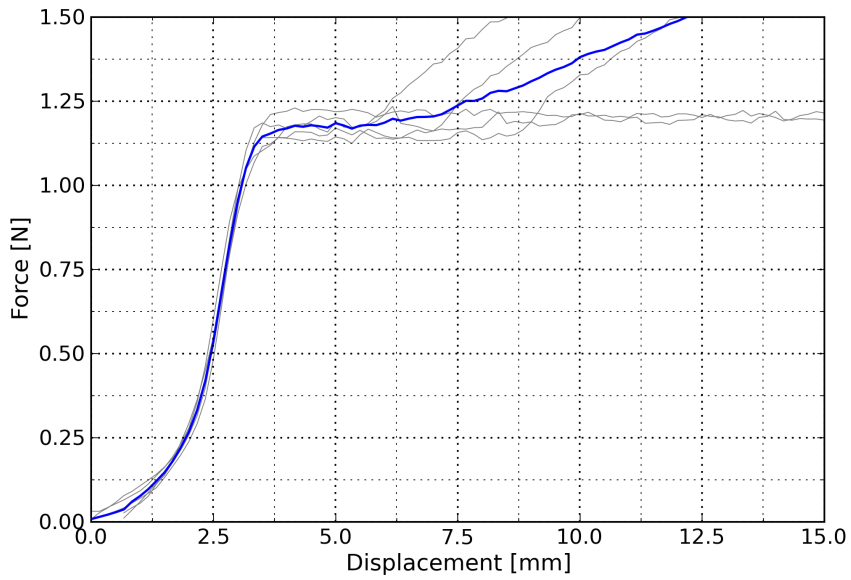
Figure A.19: Adhesion 2, 180°, M1.
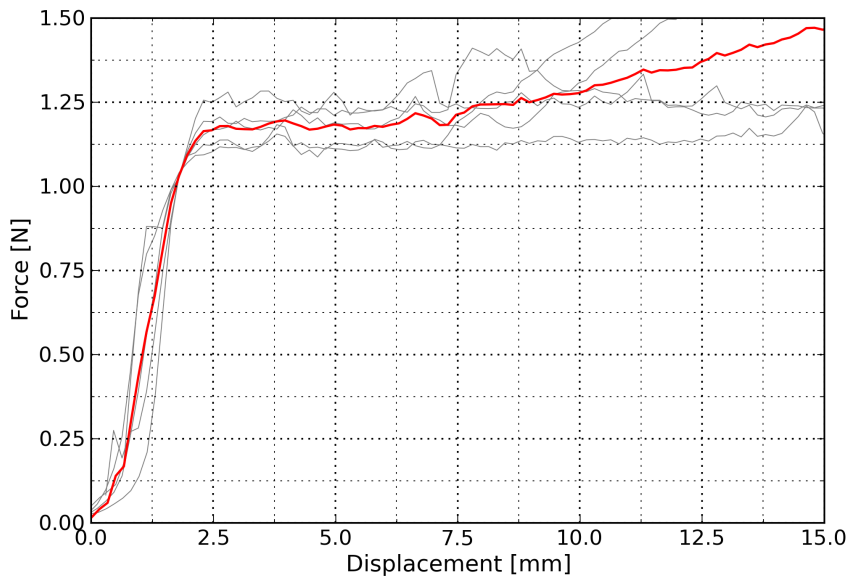
Figure A.20: Adhesion 2, 180°, M2.
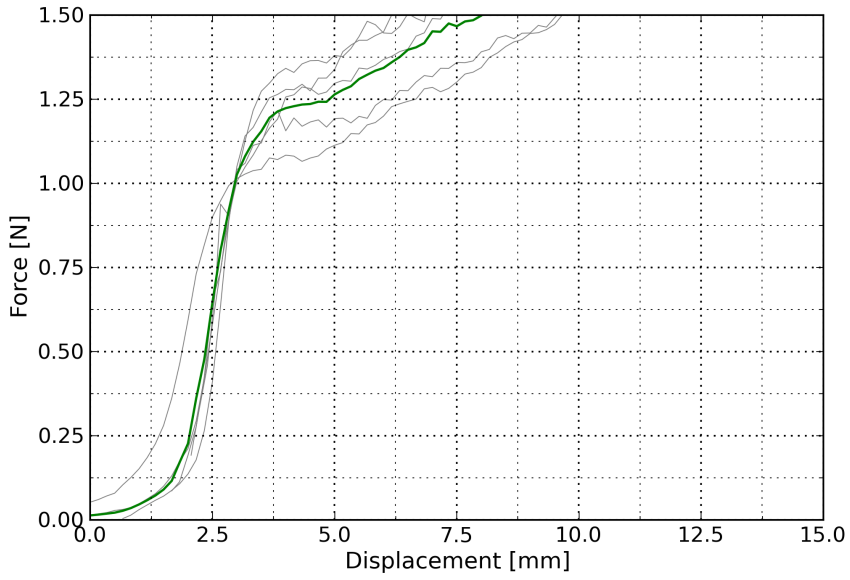
Figure A.21: Adhesion 2, 180°, M3.
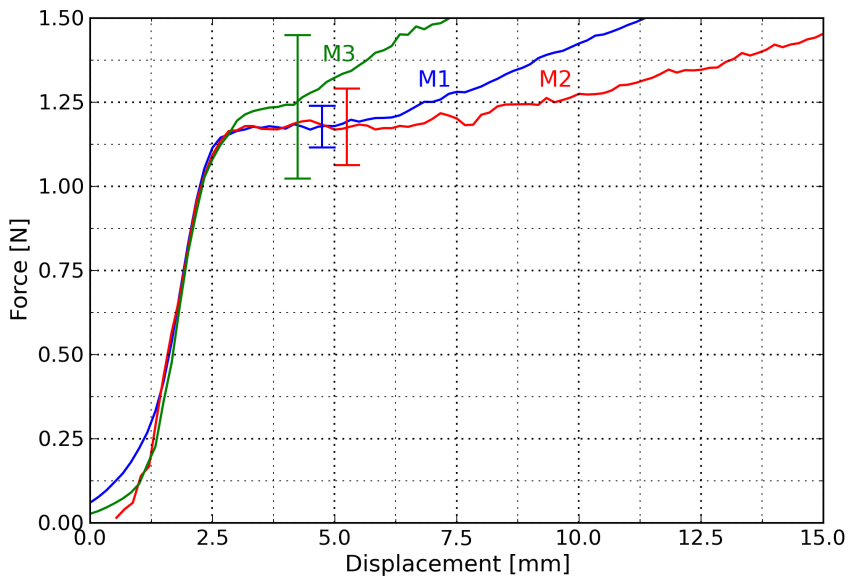
Figure A.22: Adhesion 2, 180°, mean curves.

A.3 Cross direction

A.3.1 Adhesion 1
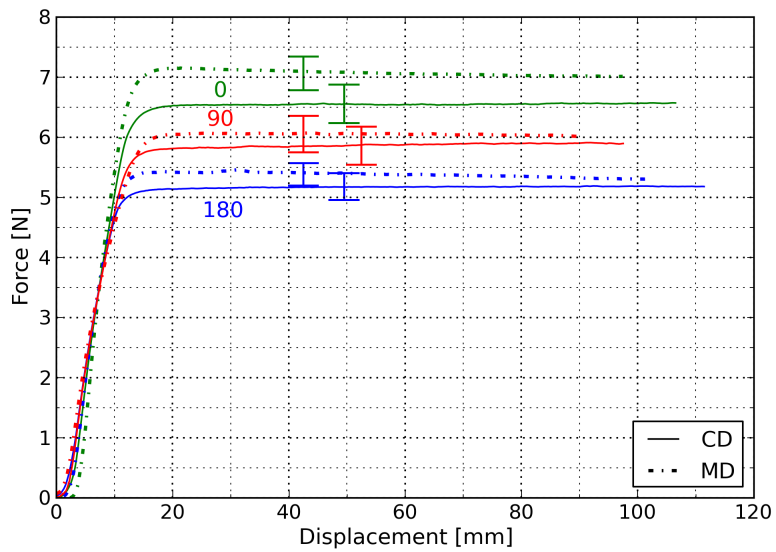
Figure A.23: Adhesion 1, M2, MD vs. CD.
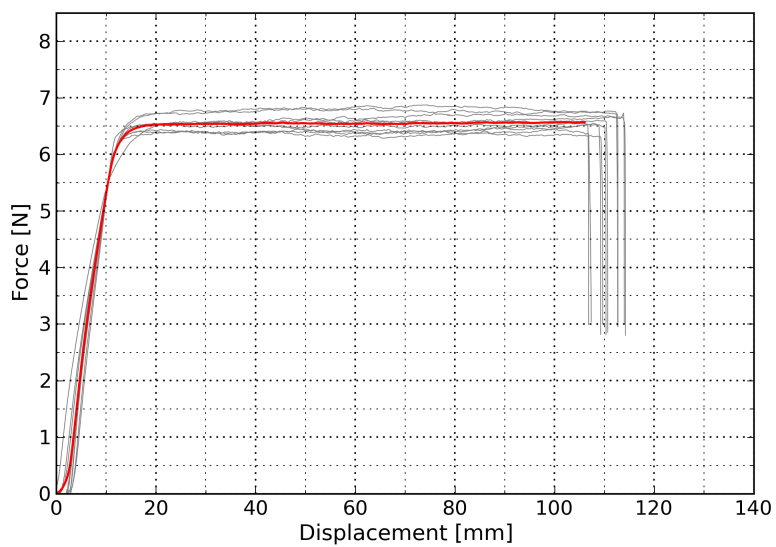
Figure A.24: Adhesion 1, 0°, M2, CD.
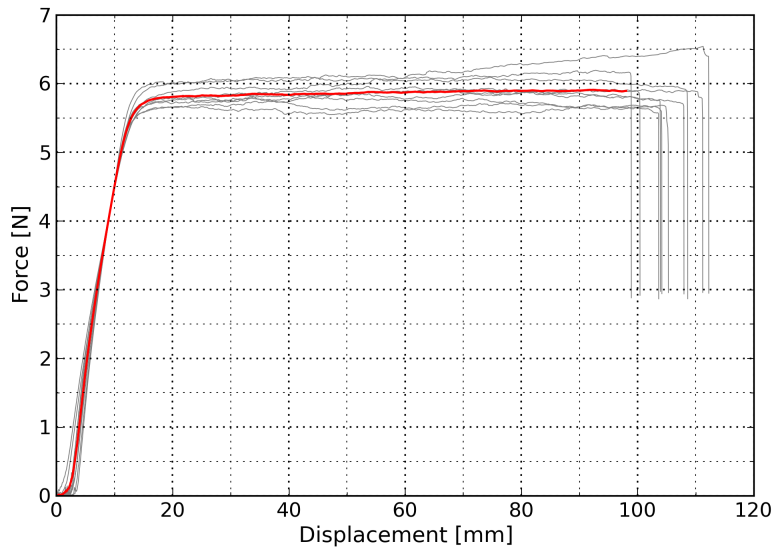
Figure A.25: Adhesion 1, 90°, M2, CD.
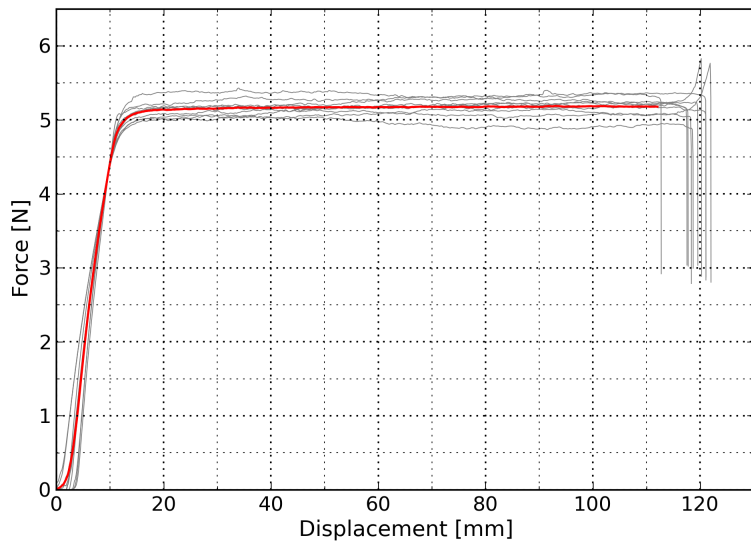
Figure A.26: Adhesion 1, 180°, M2, CD.

A.3.2 Adhesion 2
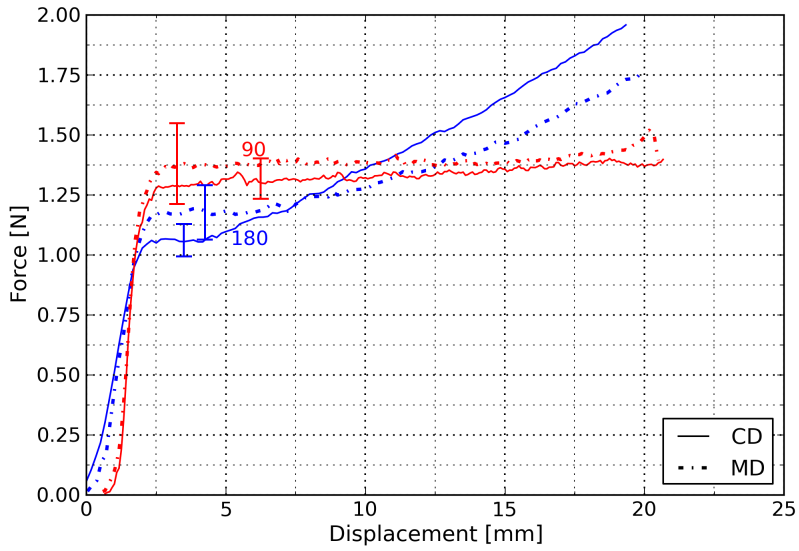
Figure A.27: Adhesion 2, M2, MD vs. CD.
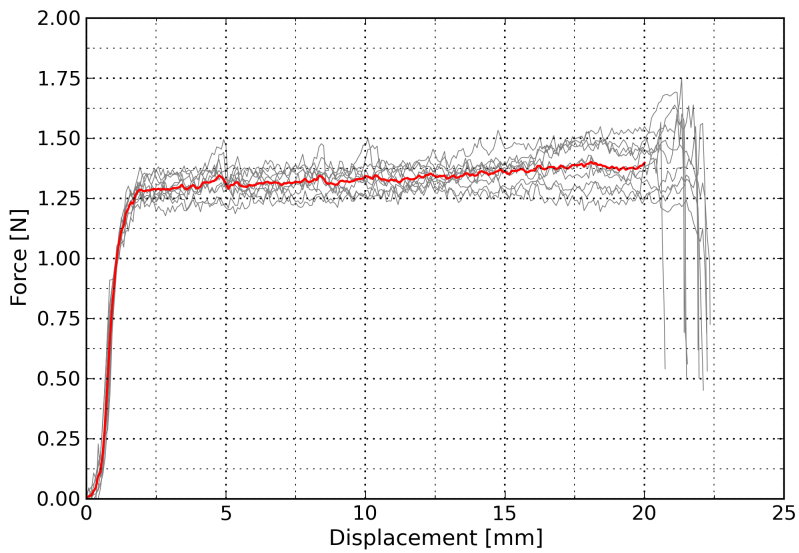

Figure A.28: Adhesion 2, 90°, M2, CD.
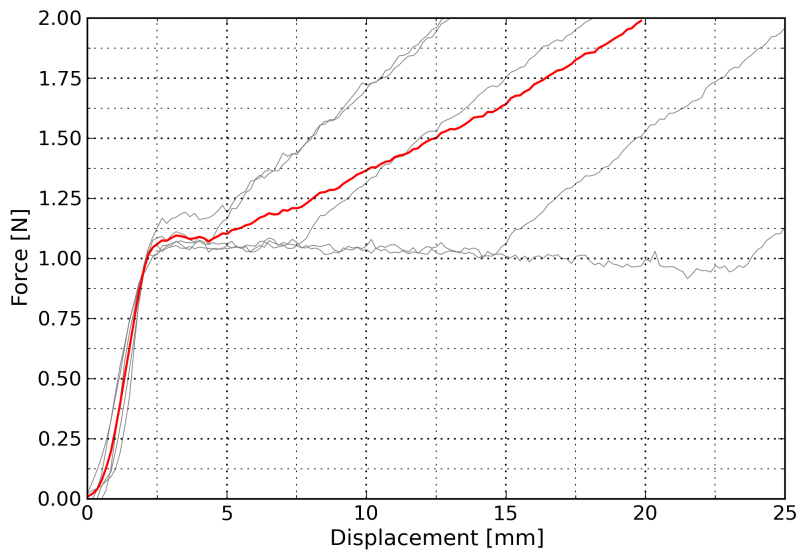
Figure A.29: Adhesion 2, 180°, M2, CD.

Appendix B

Abaqus input

```
*Instance, name=coh-1, part=coh
1.01, 0., 0.
*Node
*Element, type=COH2D4
*Nset, nset=_PickedSet2, internal, generate
1, 42, 1
*Elset, elset=_PickedSet2, internal, generate
1, 20, 1
Section:  s-coh
*Cohesive Section, elset=_PickedSet2, controls=EC-1,
material=coh-behavior, response=TRACTION SEPARATION, 14.
*End Instance


*Material, name=coh-behavior
*Damage Initiation, criterion=QUADS
15.,30.,30.
*Damage Evolution, type=ENERGY, mixed mode behavior=POWER LAW,
power=1.  0.036, 0.036, 0.036
*Elastic, type=TRACTION
40000.,80000.,80000.
```